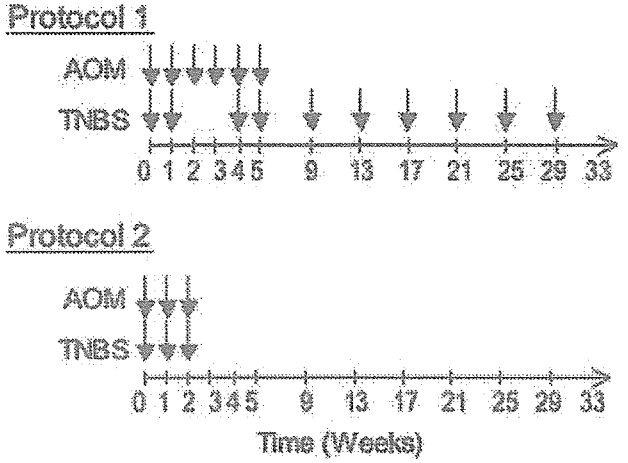

FIGURE 1 – Experimental design used in this study.

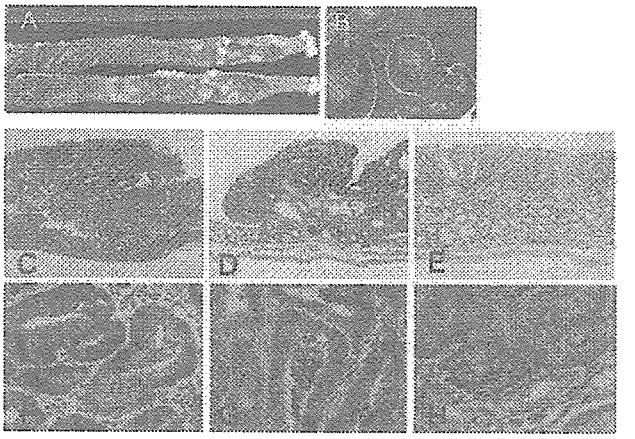

FIGURE 2 – Pathological features of colonic tumors. (*a*) Macroscopic appearance of typical tumors. Colons from IFN-$\gamma^{-/-}$ mice treated with AOM plus TNBS are shown. (*b*) Zoom stereomicroscopic appearance of tumors in panel A after staining with methylene blue. Polypoid cancer seen in WT (*c*) and IL-$4^{-/-}$ (*d*) mice treated with AOM plus TNBS, stained by H&E. (*e*) Flat-elevated cancer seen in IFN-$\gamma^{-/-}$ mice (H&E staining). Immunostaining for β-catenin of well-differentiated adenocarcinomas from WT (*f*) and IL-$4^{-/-}$ (*g*) mice showing a cell membrane pattern and moderately differentiated adenocarcinoma from IFN-$\gamma^{-/-}$ mice (*f*) showing a nuclear pattern.

Material and methods

Mice

Wild type (WT), IFN-γ gene knockout (IFN-$\gamma^{-/-}$), IL-4 gene disrupted (IL-$4^{-/-}$) mice, all on the BALB/c background were originally obtained from Jackson Laboratory (Bar Harbor, ME). The colony was maintained under pathogen-free conditions in the Immunocompromized Mouse Facility of the Research Institute, International Medical Center of Japan (IMCJ). All experiments were performed according to the Institutional Guidelines for the Care and Use of Laboratory Animals in Research and according to the approval of the local ethics committee in the IMCJ.

Induction of colitis and colon tumors

Treatment of mice was initiated when mice were 8 weeks of age. Trinitrobenzene sulfonic acid (TNBS) colitis was induced, as described previously.[19,20] A 2% solution of TNBS (Research Organics, Cleveland, OH) in PBS:ethanol (1:1 by volume) was administered intrarectally to mice, anesthetized with ketamine (Sankyo Co. Ltd., Tokyo, Japan) and xylazine (Sigma, St. Louis, MO). A dose of TNBS of 36 μg/g of body weight was given. The colon carcinogen AOM was purchased from Sigma, and a dose of 10 μg/g of body weight in saline was injected intraperitoneally. TNBS and AOM were given, as indicated (Fig. 1). In some experimental groups, treatment with either TNBS or AOM was performed. In protocol 1, six doses of AOM or 4 doses of TNBS were given during the first 5 weeks, and then TNBS was given every 4 weeks on 6 occasions, to mimic recurrence of inflammation. In protocol 2, three doses of TNBS and AOM were given together in the first 2 weeks, and colonic tissues were examined after 33 weeks. To examine the spontaneous development of tumors, some cytokine knockout mice were kept untreated, until they were 40 weeks of age.

Macroscopic and histological examination

Colonic tissues were opened longitudinally, fixed in 10% formalin overnight at 4°C, washed in PBS, stained with 2% methylene blue for contrast, and then the numbers of macroscopically visible tumors were assessed. Some specimens were examined with a zoom stereomicroscope. Tumors were removed along with the surrounding normal colonic tissues and embedded in paraffin blocks; then, 4-μm sections were prepared and stained with hematoxylin and eosin (H&E). For immunohistochemical analysis, 3-μm-thick paraffin sections were deparaffinated in xylene, rehydrated and heated at 95°C in 10 mM citrated buffer (pH 6.0) for 10 min. After treatment with 3% H_2O_2, followed by 0.25% goat serum in PBS for blocking, sections were incubated with monoclonal antibodies to p53 (DO-1, 1:200) or β-catenin (1:800, both from BD Transduction Laboratories, CA) overnight at 4°C. Mouse IgG was used as a negative control. Bound antibody was detected using Vectastain ABD-kit (Vector Laboratories, Burlingame, CA) according to vendor's protocol, and deaminobenzidine was used as substrate for peroxidase.

Statistics

The results were compared by the Mann–Whitney test or χ^2 test, using the Statview II statistical program (Abacus Concepts, Berkeley, CA) adapted for the Macintosh computer.

Results

Effects of inflammation and cytokine deficiency on the formation of colon tumors

In our study, polypoid or sessile elevated lesions were macroscopically visible in the middle to distal colon, and these were enumerated (Figs. 2*a* and 2*b*). The results of protocol 1 are summarized in Table I. When WT mice were treated with only AOM in protocol 1, 3.3 tumors/mouse were seen after 33 weeks. In IFN-$\gamma^{-/-}$ mice, the incidence of tumors induced with AOM was not significantly different from that of WT mice. IL-$4^{-/-}$ mice, treated with AOM only, did not develop tumors, except for 1 mouse with a single tumor, although aberrant crypt foci (ACF) were frequently seen by following zoom stereomicroscopy. Induction of TNBS colitis, in addition to AOM treatment, did not change the numbers of tumors in WT mice. In contrast, induction of colitis induced enhanced formation of tumors in both IFN-$\gamma^{-/-}$ and IL-$4^{-/-}$ mice. Of note, the number of tumors in IFN-$\gamma^{-/-}$ mouse reached to 8 tumors/mouse, which was significantly higher when compared with those in IL-$4^{-/-}$ or WT mice. The incidence of tumor bearing mice was 100% in the IFN-$\gamma^{-/-}$ group. There were no significant differences in the size of the tumors, which developed in each experimental group. In protocol 1, most of the deaths occurred mostly in the first 8 weeks. The exceptions were that some IL-$4^{-/-}$ mice treated with TNBS died in later period, coinciding with our previous report that IL-$4^{-/-}$ mice are more susceptible to TNBS colitis.[19] Further, we did not see any tumors in the mice which died before 33 weeks, including IL-$4^{-/-}$ mice.

TABLE I – NUMBER OF TUMORS IN CYTOKINE DEFICIENT MICE (PROTOCOL 1)

Mice	Treatment	No. of mice survived/total	Incidence of tumor	No. of tumors/mouse	Size of tumors (mm^3)	Total number of tumors
WT	AOM	7/12 (58)[1]	5/7 (71)	3.3 ± 2.9	2.2 ± 1.3	23
WT	AOM + TNBS	10/17 (59)	6/10 (60)	2.0 ± 2.5	2.9 ± 1.3	20
WT	TNBS	5/5 (100)	0/5 (0)	0 ± 0		0
IFN-$\gamma^{-/-}$	AOM	7/16 (43)	2/7 (28)	1.4 ± 2.3	2.7 ± 1.9	10
IFN-$\gamma^{-/-}$	AOM + TNBS	7/11 (64)	7/7 (100)[2]	8.3 ± 1.8[3]	2.8 ± 1.8	58
IFN-$\gamma^{-/-}$	TNBS	8/10 (80)	0/8 (0)	0 ± 0		0
IFN-$\gamma^{-/-}$	Untreated	8/8 (100)	0/8 (0)	0 ± 0		0
IL-$4^{-/-}$	AOM	15/17 (88)	1/15 (7)	0.1 ± 0.3[4]	1.6	1
IL-$4^{-/-}$	AOM+TNBS	7/11 (64)	5/7 (71)[5]	3.1 ± 3.4	1.7 ± 1.2	22
IL-$4^{-/-}$	TNBS	2/7 (29)	0/2 (0)	0 ± 0		0
IL-$4^{-/-}$	Untreated	4/4 (100)	0/4 (0)	0 ± 0		0

[1]Values in parentheses indicate percentages.–[2]Difference from IFN-$\gamma^{-/-}$ or IL-$4^{-/-}$ mice treated AOM was statistically significant ($p<0.02$).–[3]Differences from all other experimental groups were statistically significant ($p < 0.02$).–[4]Differences from WT mice with AOM or AOM+TNBS were statistically significant ($p<0.02$).–[5]Difference from IL-$4^{-/-}$ mice treated AOM was statistically significant ($p < 0.02$).

TABLE II – NUMBERS OF TUMORS IN CYTOKINE DEFICIENT MICE (PROTOCOL 2)

Mice	Treatment	No. of mice survived/total	Incidence of tumor formation	No. of tumors/mouse	Total number of tumors
IFN-$\gamma^{-/-}$	AOM + TNBS	19/24 (79)[1]	10/19[2] (53)	0.8 ± 0.9[2]	15
IL-$4^{-/-}$	AOM + TNBS	12/24 (50)	0/12 (0)	0	0

[1]Values in parentheses indicate percentages.–[2]Differences from IL-$4^{-/-}$ mice were statistically significant ($p < 0.02$).

It indicated that mortality was not associated with cancer, but more with susceptibility to TNBS colitis or toxicity of AOM in each mouse strain.

Next, to conform the difference between IL-$4^{-/-}$ and IFN-$\gamma^{-/-}$ mice treated with both AOM and TNBS, we have chosen protocol 2 (Fig. 1), reducing the dose of AOM and TNBS. A change in the dose of AOM improved the survival of IFN-$\gamma^{-/-}$ mice; however, this dose change did not affect the survival of IL-$4^{-/-}$ mice, probably because of their higher sensitivity to TNBS colitis than IFN-$\gamma^{-/-}$ mice (Table II). In this protocol, death occurred within the first 3 weeks, and no tumor-caused death was observed in both groups. Although the numbers of tumor/mouse decreased in this protocol, we saw similar differences between the IFN-$\gamma^{-/-}$ and IL-$4^{-/-}$ mice groups (Table II). No visible tumors were seen in IL-$4^{-/-}$ mice. In contrast, 10 of 19 IFN-$\gamma^{-/-}$ mice formed more than 1 tumor in the colon.

Microscopic findings

Tumors formed in protocol 1 were subjected to microscopic examination. The majority of these were polypoid lesions (Figs. 2*c* and 2*d*), and some of them were flat, elevated lesions (Fig. 2*e*). Tumors histologically examined were all diagnosed as well-differentiated or moderately differentiated adenocarcinoma. There was also colonic dysplasia involving 1–2 crypts, in mouse groups that had treatment with AOM. In each groups of mice, there were no differences in the severity of cell infiltration into tumors. In IFN-$\gamma^{-/-}$ mice with TNBS colitis, deformity of crypts was the most evident, as previously reported[20]; however, there were no clear relations to tumor location. In WT mice, the ratio of moderately differentiated adenocarcinoma from mice treated with both AOM and TNBS tended to be higher than those treated only with AOM, in which well-differentiated adenocarcinoma was the major type (Fig. 3). The majority of tumors from IFN-$\gamma^{-/-}$ mice were moderately differentiated adenocarcinomas in both AOM or AOM plus TNBS treated groups (Fig. 3). In protocol 2, fourteen out of 15 tumors from IFN-$\gamma^{-/-}$ mice treated with AOM plus TNBS were also diagnosed as moderately differentiated adenocarcinomas. One tumor was a well-differentiated adenocarcinoma.

Immunohistochemistry

Immunostaining for p53 and β-catenin was performed. Staining with anti-p53 monoclonal antibody was generally weak, and obviously enhanced nuclear staining was seen in only 2 tumors in IFN-$\gamma^{-/-}$ mice treated with AOM plus TNBS, 2 from IL-$4^{-/-}$ mice

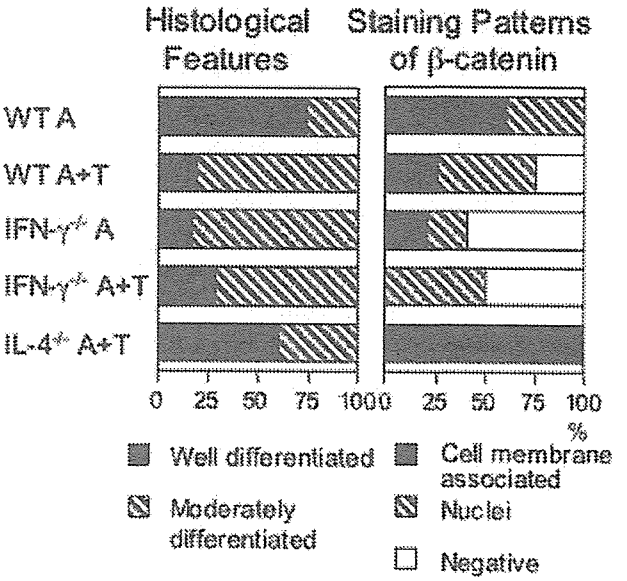

FIGURE 3 – Percentage of histological diagnosis and β-catenin staining pattern of colon tumors. Tumors (6–10) from each mouse group in protocol 1 were evaluated for their histological grading and expression of β-catenin. A, treated with AOM; T, treated with TNBS.

treated with AOM plus TNBS and 2 tumors from WT mice treated with AOM (data not shown). In contrast, a differential staining pattern with β-catenin was seen. Well-differentiated adenocarcinomas in WT and IL-$4^{-/-}$ mice showed typical staining of cell membrane, which was much stronger than that in normal epithelial cells (Figs. 2*f* and 2*g*). In contrast, nuclear staining was frequently observed in tumors from IFN-$\gamma^{-/-}$ mice treated with AOM plus TNBS (Fig. 2*h*). All tumors from IL-$4^{-/-}$ mice showed a cell membrane pattern, including the one from mice treated with only AOM. There was no tumor with a membrane-staining pattern from IFN-$\gamma^{-/-}$ mice treated with AOM plus TNBS (Fig. 3). Thus, nuclear and membrane localization of β-catenin was the characteristics of moderately differentiated adenocarcinomas in IFN-$\gamma^{-/-}$ mice and well-differentiated adenocarcinoma in IL-$4^{-/-}$ mice, respectively (Fig. 3).

Discussion

In the present study comparing WT, IFN-$\gamma^{-/-}$ and IL-$4^{-/-}$ mice, several new findings in colitis-related colon cancer were revealed. First, in the absence of IFN-γ, induction of TNBS colitis and AOM strongly enhanced tumor formation in the colon. Importantly, colitis also affected the histological degree of differentiation, and frequently induced nuclear translocation of β-catenin.

Although the precise mechanism of enhancement of tumor formation is not yet clear, one possibility is that a defect of tumor immunosurveillance occurs in IFN-$\gamma^{-/-}$ mice. Previous studies showed that IFN-$\gamma^{-/-}$ mice develop chemical carcinogen methylcholanthrene-induced sarcoma,[25] spontaneous lymphomas and lung adenocarcinomas[26] more frequently than do WT mice. In our studies, there were no significant differences in the frequency of tumor formation between WT and IFN-$\gamma^{-/-}$ mice, when inflammation was not induced. In contrast, in the presence of colitis, the number of tumors in IFN-$\gamma^{-/-}$ mice was markedly increased, while tumor frequency in WT mice was not increased. This result in WT mice is distinct from studies reporting the development of AOM-induced tumors within a short term in WT mice when DSS colitis was induced,[27,28] although there has been no report testing IFN-$\gamma^{-/-}$ mice. In DSS colitis, diffuse loss of epithelium is the primary pathological finding, which might increase the chance of carcinogenesis and promotion during vigorous epithelial cell regeneration. On the other hand, since TNBS colitis is characterized by a focal ulcer and a strong hapten (trinitrophenyl residue)-specific immune response of T and B cells, IFN-γ produced as a part of adoptive immunity in the inflammation seems to be important for protection from the colonic tumor. In other words, IFN-γ production may not be required for tumor surveillance in non-inflamed, steady state colons of BALB/c mice. A significant incidence of lung carcinoma, but no report of colon carcinoma during the life span of more than 600 days in BALB/c IFN-$\gamma^{-/-}$ mice, also supports this notion.[26] The importance of IFN-γ in tumor surveillance produced by T cells as a part of adoptive immunity was also shown in the previous study that RAG2$^{-/-}$ x STAT1$^{-/-}$ double knockout mice showed increased susceptibly to methylcholanthrene-induced carcinogenesis, but did not display a significantly greater tumor incidence, when compared with mice that lacked either RAG2 or STAT1 genes.[25] Thus, it is feasible that the colonic mucosa of UC, which fails to induce prevailing upregulation of IFN-γ but produces Th2-type cytokines, can frequently develop colonic carcinoma. On the other hand, our results also showed that addition of TNBS colitis to AOM increased the incidence of tumor in IL-$4^{-/-}$ mice, although the number was much less than in IFN-$\gamma^{-/-}$ mice. This result suggested that aberrant Th1-dominant inflammatory responses might also increase the tumor risk, although it was not comparable to that in Th2 dominant condition.

Since there is an interaction between Th1 and Th2 cytokines that they suppress the effect of each other, the presence of an excess amount of Th2 cytokines in IFN-$\gamma^{-/-}$ would have a significant effect. We have previously analyzed the cytokine production by colonic CD4$^+$ cells in WT, IL-$4^{-/-}$ and IFN-$\gamma^{-/-}$ mice in naïve colon, as well as in acute (day 1) and chronic (day 10) phase of TNBS colitis. Colonic CD4$^+$ T cells from IFN-$\gamma^{-/-}$ mice produced very large amounts of IL-4 and IL-5. In contrast, secretion of IFN-γ by colonic CD4$^+$ T cells from IL-$4^{-/-}$ mice was higher than in colonic CD4$^+$ T cells from WT mice.[19,20] In protocol 1 of current study, the number of tumors in IL-$4^{-/-}$ mice was much lower than those of WT or IFN-$\gamma^{-/-}$ mice. In protocol 2, none of the IL-$4^{-/-}$ mice developed tumors, in contrast to the 53% incidence in IFN-$\gamma^{-/-}$ mice. These results suggest that IL-4 may have a direct effect on promoting tumor formation. In fact, many malignant tumors express the IL-4 receptor, which is able to bind to both IL-4 and IL-13 and also the high affinity decoy receptor of IL-13, IL-13 receptor α2.[29] However, the function of IL-4 and IL-13 in tumor cells, especially in colonic cancer is not yet clear, and the output effect via these receptors still remains to be investigated. Early studies showed that IL-4 and IL-13 had antitumor activity in mice by growth inhibition[30] through IL-4 receptor.[31] However, subversion of host antitumor defenses has also been demonstrated for IL-13. Recent studies using tumor cell lines demonstrated that STAT6, IL-4 and IL-13 were capable of inhibiting tumor rejection.[32–34] Thus, Th2 type cytokines appear to antagonize tumor immunosurveillance.

In our study, IL-$4^{-/-}$ mice and IFN-$\gamma^{-/-}$ mice showed distinct expression patterns for β-catenin, cell membrane and nuclear staining in IL-$4^{-/-}$ and IFN-$\gamma^{-/-}$ mice, respectively, while WT mice had tumors of both patterns. This again suggests that Th2-cytokine predominance directly influences the mutation of DNA in epithelial cells. Indeed, exogenous IL-4 and IL-13 decreased the levels of membrane staining of β-catenin in keratinocytes, without changes of total protein levels of β-catenin, while IFN-γ enhanced membrane staining.[35] In our model, gene mutation induced by AOM might facilitate nuclear translocation of β-catenin, which had localized in cytoplasm, but not in cell membrane by the action of IL-4 and IL-13, secreted as inflammatory responses of IFN-$\gamma^{-/-}$ mice. Thus, we propose that enhancement of tumor formation in IFN-$\gamma^{-/-}$ mice is due both to a lack of immunosurveillance by IFN-γ and promotion of carcinogenesis by excess Th2 type cytokines. In this context, epithelial cells in the process of tissue repair in the inflamed colon are susceptible to the absence of IFN-γ and the presence of excess amount of IL-4 and IL-13.

In summary, our results show that a predominance of Th2 type cytokines in the inflamed colon, which mimics mucosal immunity in UC, promotes aberrant β-catenin expression and tumor formation. This model will be useful to further clarify the mechanism of colitic-cancer and for our search for targets or new agents for prevention of colon cancer.

References

1. Eaden JA, Abrams KR, Mayberry JF. The risk of colorectal cancer in ulcerative colitis: a meta-analysis. Gut 2001;48:526–35.
2. Allison M, Dhillon A, Lewis W, Pounder R, eds. Inflammatory bowel disease. London: Mosby, 1998. 111–19.
3. Gyde SN, Prior P, Allan RN, Stevens A, Jewell DP, Truelove SC, Lofberg R, Brostrom O, Hellers G. Colorectal cancer in ulcerative colitis: a cohort study of primary referrals from three centres. Gut 1988;29:206–17.
4. Balkwill F, Mantovani A. Inflammation and cancer: back to Virchow? Lancet 2001;357:539–45.
5. Cooper HS, Murthy S, Kido K, Yoshitake H, Flanigan A. Dysplasia and cancer in the dextran sulfate sodium mouse colitis model. Relevance to colitis-associated neoplasia in the human: a study of histopathology, B-catenin and p53 expression and the role of inflammation. Carcinogenesis 2000;21:757–68.
6. Hirono I, Kuhara K, Hosaka S, Tomizawa S, Golberg L. Induction of intestinal tumors in rats by dextran sulfate sodium. J Natl Cancer Inst 1981;66:579–83.
7. Yamada M, Ohkusa T, Okayasu I. Occurrence of dysplasia and adenocarcinoma after experimental chronic ulcerative colitis in hamsters induced by dextran sulphate sodium. Gut 1992;33:1521–7.
8. Pikarsky E, Porat RM, Stein I, Abramovitch R, Amit S, Kasem S, Gutkovich-Pyest E, Urieli-Shoval S, Galun E, Ben-Neriah Y. NF-kappaB functions as a tumour promoter in inflammation-associated cancer. Nature 2004;431:461–6.
9. Greten FR, Eckmann L, Greten TF, Park JM, Li ZW, Egan LJ, Kagnoff MF, Karin M. IKKbeta links inflammation and tumorigenesis in a mouse model of colitis-associated cancer. Cell 2004;118: 285–96.
10. Day DW, Jass JR, Price AB, Shepherd NA, Sloan JM, Talbot IC, Warren BF, Williams GT, eds. Morson and Dawson's gastrointestinal pathology. Oxford: Blackwell, 2003. 472–539.
11. Lashner BA, Shapiro BD, Husain A, Goldblum JR. Evaluation of the usefulness of testing for p53 mutations in colorectal cancer surveillance for ulcerative colitis. Am J Gastroenterol 1999;94:456–62.
12. Ilyas M, Talbot IC. p53 expression in ulcerative colitis: a longitudinal study. Gut 1995;37:802–4.
13. Yin J, Harpaz N, Tong Y, Huang Y, Laurin J, Greenwald BD, Hontanosas M, Newkirk C, Meltzer SJ. p53 point mutations in dysplastic

and cancerous ulcerative colitis lesions. Gastroenterology 1993;104: 1633–9.
14. Brentnall TA, Crispin DA, Rabinovitch PS, Haggitt RC, Rubin CE, Stevens AC, Burmer GC. Mutations in the p53 gene: an early marker of neoplastic progression in ulcerative colitis. Gastroenterology 1994; 107:369–78.
15. Parronchi P, Romagnani P, Annunziato F, Sampognaro S, Becchio A, Giannarini L, Maggi E, Pupilli C, Tonelli F, Romagnani S. Type 1 T-helper cell predominance and interleukin-12 expression in the gut of patients with Crohn's disease. Am J Pathol 1997;150:823–32.
16. Kakazu T, Hara J, Matsumoto T, Nakamura S, Oshitani N, Arakawa T, Kitano A, Nakatani K, Kinjo F, Kuroki T. Type 1 T-helper cell predominance in granulomas of Crohn's disease. Am J Gastroenterol 1999;94:2149–55.
17. Fuss IJ, Neurath M, Boirivant M, Klein JS, de la Motte C, Strong SA, Fiocchi C, Strober W. Disparate $CD4^+$ lamina propria (LP) lymphokine secretion profiles in inflammatory bowel disease. Crohn's disease LP cells manifest increased secretion of IFN-gamma, whereas ulcerative colitis LP cells manifest increased secretion of IL-5. J Immunol 1996;157:1261–70.
18. Inoue S, Matsumoto T, Iida M, Mizuno M, Kuroki F, Hoshika K, Shimizu M. Characterization of cytokine expression in the rectal mucosa of ulcerative colitis: correlation with disease activity. Am J Gastroenterol 1999;94:2441–6.
19. Dohi T, Fujihashi K, Kiyono H, Elson CO, McGhee JR. Mice deficient in Th1- and Th2-type cytokines develop distinct forms of hapten-induced colitis. Gastroenterology 2000;119:724–33.
20. Dohi T, Fujihashi K, Rennert PD, Iwatani K, Kiyono H, McGhee JR. Hapten-induced colitis is associated with colonic patch hypertrophy and T helper 2-type responses. J Exp Med 1999;189:1169–80.
21. Heller F, Fuss IJ, Nieuwenhuis EE, Blumberg RS, Strober W. Oxazolone colitis, a Th2 colitis model resembling ulcerative colitis, is mediated by IL-13-producing NK-T cells. Immunity 2002;17:629–38.
22. Boirivant M, Fuss IJ, Chu A, Strober W. Oxazolone colitis: a murine model of T helper cell type 2 colitis treatable with antibodies to interleukin 4. J Exp Med 1998;188:1929–39.
23. Dohi T, Fujihashi K, Koga T, Shirai Y, Kawamura YI, Ejima C, Kato R, Saitoh K, McGhee JR. T helper type-2 cells induce ileal villus atrophy, goblet cell metaplasia and wasting disease in T cell-deficient mice. Gastroenterology 2003;124:672–82.
24. Dohi T, Fujihashi K, Koga T, Etani Y, Yoshino N, Kawamura YI, McGhee JR. $CD4^+CD45RB^{Hi}$ inteleukin-4 defective T cells elicit antral gastritis and duodenitis. Am J Pathol 2004;165:1257–68.
25. Shankaran V, Ikeda H, Bruce AT, White JM, Swanson PE, Old LJ, Schreiber RD. IFNgamma and lymphocytes prevent primary tumour development and shape tumour immunogenicity. Nature 2001;410: 1107–11.
26. Street SE, Trapani JA, MacGregor D, Smyth MJ. Suppression of lymphoma and epithelial malignancies effected by interferon gamma. J Exp Med 2002;196:129–34.
27. Tanaka T, Kohno H, Suzuki R, Yamada Y, Sugie S, Mori H. A novel inflammation-related mouse colon carcinogenesis model induced by azoxymethane and dextran sodium sulfate. Cancer Sci 2003;94:965–73.
28. Becker C, Fantini MC, Schramm C, Lehr HA, Wirtz S, Nikolaev A, Burg J, Strand S, Kiesslich R, Huber S, Ito H, Nishimoto N, et al. TGF-beta suppresses tumor progression in colon cancer by inhibition of IL-6 trans-signaling. Immunity 2004;21:491–501.
29. Wynn TA. IL-13 effector functions. Annu Rev Immunol 2003;21: 425–56.
30. Puri R. Structure and function of interleukin 4 and its receptors. In: Kurzrock R, Talpaz M, eds. Cytokines: interleukins and their receptors. Norwell: Kluwer, 1995.143–85.
31. Renard N, Duvert V, Banchereau J, Saeland S. Interleukin-13 inhibits the proliferation of normal and leukemic human. Blood 1994;84: 2253–60.
32. Ostrand-Rosenberg S, Grusby MJ, Clements VK. Cutting edge: STAT6-deficient mice have enhanced tumor immunity to primary and metastatic mammary carcinoma. J Immunol 2000;165:6015–19.
33. Kacha AK, Fallarino F, Markiewicz MA, Gajewski TF. Cutting edge: spontaneous rejection of poorly immunogenic P1.HTR tumors by Stat6-deficient mice. J Immunol 2000;165:6024–8.
34. Terabe M, Matsui S, Noben-Trauth N, Chen H, Watson C, Donaldson DD, Carbone DP, Paul WE, Berzofsky JA. NKT cell-mediated repression of tumor immunosurveillance by IL-13 and the IL-4R-STAT6 pathway. Nat Immunol 2000;1:515–20.
35. Fujii-Maeda S, Kajiwara K, Ikizawa K, Shinazawa M, Yu B, Koga T, Furue M, Yanagihara Y. Reciprocal regulation of thymus and activation-regulated chemokine/macrophage-derived chemokine production by interleukin (IL)-4/IL-13 and interferon-gamma in HaCaT keratinocytes is mediated by alterations in E-cadherin distribution. J Invest Dermatol 2004;122:20–8.

Available online at www.sciencedirect.com
SCIENCE DIRECT
ELSEVIER
Cancer Letters 236 (2006) 32–38
CANCER Letters
www.elsevier.com/locate/canlet

Parp-1 deficiency does not enhance liver carcinogenesis induced by 2-amino-3-methylimidazo[4,5-*f*]quinoline in mice

Kumiko Ogawa[a,*], Mitsuko Masutani[b], Koji Kato[a], Mingxi Tang[a], Nobuo Kamada[c], Hiroshi Suzuki[d], Hitoshi Nakagama[b], Takashi Sugimura[b], Tomoyuki Shirai[a]

[a]*Department of Experimental Pathology and Tumor Biology, Nagoya City University, Graduate School of Medical Sciences, Nagoya 467-8601, Japan*
[b]*Biochemistry Division, National Cancer Center Research Institute, 1-1 Tsukiji 5-chome, Chuo-ku, Tokyo 104-0045, Japan*
[c]*Chugai Pharmaceutical Co., Ltd, Gotemba, Shizuoka 412-8513, Japan*
[d]*National Research Center for Protozoan Diseases, Obihiro University of Agriculture and Veterinary Medicine, Obihiro, Hokkaido 080-8555, Japan*

Received 11 February 2005; received in revised form 25 April 2005; accepted 28 April 2005

Abstract

The susceptibility of poly(ADP-ribose) polymerase-1 (Parp-1) knockout mice to 2-amino-3-methylimidazo[4,5-*f*]quinoline (IQ)-induced liver carcinogenesis was analyzed. Twelve-week-old male *Parp-1*$^{+/+}$, *Parp-1*$^{+/-}$ and *Parp-1*$^{-/-}$ mice of the C57BL/6 congenic strain were fed a diet containing IQ at a concentration of 300 ppm or a control diet for 60 weeks. Hepatocellular carcinomas were observed only in 1/19, 2/18 and 1/17 of the *Parp-1*$^{-/-}$, *Parp-1*$^{+/-}$ and *Parp-1*$^{+/+}$ mice, respectively. *Parp-1* deficiency did not affect the susceptibility of mice to carcinogenicity of IQ, which produces bulky DNA adducts that are repaired mainly through the nucleotide excision repair pathway. This result is in sharp contrast to the increased susceptibility of *Parp-1*$^{-/-}$ mice to carcinogenesis induced by alkylating agents that produce DNA damage repaired mainly through base excision repair and DNA strand break repair pathways.

Keywords: PARP; IQ; Knockout mice; Liver; Carcinogenesis

1. Introduction

Cellular DNA damage is constantly generated by physical and chemical stimuli from the environment, such as ultraviolet (UV) radiation, exhaust fumes, as well as many chemicals in foods, and various systems of DNA repair have evolved which prevent mutations and thus tumor induction.

Poly(ADP-ribose) polymerase-1 (Parp-1) has multiple functions in DNA repair/recombination [1], maintenance of genomic stability [2,3], and induction of cell death accompanying nicotinamide adenine dinucleotide (NAD) depletion [4,5]. Parp-1 is also involved in transcriptional regulation and control of

* Corresponding author. Tel.: +81 52 853 8156; fax: +81 52 842 0817.
E-mail address: kogawa@med.nagoya-cu.ac.jp (K. Ogawa).

0304-3835/$ - see front matter © 2005 Elsevier Ireland Ltd. All rights reserved.
doi:10.1016/j.canlet.2005.04.030

differentiation [6–8] and thus may play important roles in preventing carcinogenesis [9]. Among the five major DNA repair pathways [10], accumulating evidence suggests that Parp-1 contributes mainly to base excision repair (BER) [2,11] as well as single- and double-strand break repair [12,13]. In *Parp-1* knockout mice disrupted in *Parp-1* exon 1 [14], increased sensitivity regarding *N*-nitrosobis(2-hydroxypropyl)amine (BHP)-induction of liver hemangiomas and hemangiosarcomas [15] and azoxymethane-induced colon and liver tumors [16] has been demonstrated. Although spontaneous tumors were not observed at 7 and 9 months of age in mice having an ICR:129/Sv mixed genetic background [15,16], the incidences of hepatocellular carcinomas were increased at 18–24 months of age with a 129/Sv: 129/Ev:C57BL/6: albino mixed genetic background [17], and in the ICR:129/Sv case [18]

In the present study, to clarify the impact of *Parp-1* deficiency on carcinogenesis induced by a different type of chemical, the susceptibility of *Parp-1* knockout mice to the carcinogenic activity of 2-amino-3-methylimidazo[4,5-*f*]quinoline (IQ), a mutagenic and carcinogenic heterocyclic amine [19] produced during cooking of meat and fish [20], was analyzed. After enzymatic activation, IQ produces bulky adducts in DNA which have been suggested to be repaired mainly through nucleotide excision repair (NER) [21], in contrast to the case of alkylating agents, especially methylating agents, in which the induced lesions are repaired mostly through BER [22] and DNA strand break repair. Comparison of the results of tumorigenesis induced by IQ and alkylating agents may provide useful information to elucidate the impact of *Parp-1* deficiency on DNA repair in relation to carcinogenesis.

2. Materials and methods

2.1. Animals and chemicals

Parp-1 knockout mice were generated by disrupting the *Parp-1* exon 1 through insertion of a neomycin resistance gene cassette [14] and then serial backcross mating was carried out to establish a C57BL/6 congenic strain [23]. Eleven-week-old male wild type (*Parp-1*$^{+/+}$), hetero (*Parp-1*$^{+/-}$) and null (*Parp-1*$^{-/-}$) littermate male mice were produced by in vitro fertilization and housed, five to a cage on wood-chip bedding, in an air-conditioned animal room targeted to 23±2 °C and 50% humidity. Food and water were available *ad libitum* throughout the experiment. Body weights were measured weekly. Use of the animals in carcinogenesis experiments was conducted according to the Guidelines for the Care and Use of Laboratory Animals of Nagoya City University Graduate School of Medical Sciences, and was approved by the Institutional Animal Care and Use Committee. The animals were also treated in accordance with the Guiding Principles for the Care and Use of Laboratory Animals of other participating institutions. IQ was dissolved in ethanol and added at 300 ppm to powdered CE2 diet (CLEA JAPAN, Tokyo, Japan), which was then pelleted at 100 °C for a few seconds and dried at 70 °C for 2 h. The presence of approximately 100% of the initial dose of IQ in the IQ-containing diet one year after its preparation was confirmed by HPLC after extraction with methanol, as described elsewhere [19].

2.2. Treatment and analysis

After a one-week initial observation period with the control diet, starting from the 12 weeks of age, the IQ-containing diet was given to mice of groups 1–3 (20 mice each for *Parp-1*$^{+/+}$, *Parp-1*$^{+/-}$ and *Parp-1*$^{-/-}$). Groups 4–6 (6, 10, 8 mice each for *Parp-1*$^{+/+}$, *Parp-1*$^{+/-}$ and *Parp-1*$^{-/-}$) received the control diet. All surviving mice were killed under ether anesthesia at the end of experimental week 60. Most of the animals killed upon becoming moribund were also analyzed. After a careful and gross examination, liver, kidneys and spleen were removed and weighed. Macroscopic lesions, and liver, kidneys, spleen, lungs, stomach and brain were fixed in buffered 10% formalin, trimmed and routinely embedded in paraffin. Sections cut at 3 μm thickness were stained with hematoxylin and eosin for histological examination.

2.3. Statistical analysis

Kruskal–Wallis and Bonferroni/Dunn analysis was used for statistical analysis of the quantitative data and χ^2 analysis was performed for the incidence data.

3. Results

Initial mean body weights of the *Parp-1*$^{-/-}$ mice (24.7 ± 1.8 g) were significantly lower than those of their *Parp-1*$^{+/+}$ (27.1 ± 2.4 g) and *Parp-1*$^{+/-}$ (27.3 ± 2.2 g) counterparts, at $P < 0.001$. Body weight gain and relative kidney weights were apparently suppressed by IQ in all genotypes (Table 1). Food consumption of the mice per body weight on the IQ-containing diet was lower than with the control diet, but no variation was observed among the different genotypes (data not shown). All of the control diet and 85, 80, and 85% of *Parp-1*$^{+/+}$, *Parp-1*$^{+/-}$, and *Parp-1*$^{-/-}$ mice, respectively, given IQ survived until the termination of the experiment. Final body weights and relative kidney and spleen weights in the *Parp-1*$^{-/-}$ mice receiving IQ were significantly lower than those of *Parp-1*$^{+/+}$ mice ($P < 0.01$, 0.001 and 0.01, respectively). Final body weights and relative kidney weights were also lower in *Parp-1*$^{-/-}$ than *Parp-1*$^{+/+}$ controls, although the difference was not significant. Relative liver weights in *Parp-1*$^{+/+}$ mice given IQ were significantly higher than those in *Parp-1*$^{+/+}$ mice given the control diet ($P < 0.01$).

Liver nodules were observed macroscopically in two *Parp-1*$^{+/-}$ and one *Parp-1*$^{-/-}$ mice treated with IQ that became moribund before the termination of the experiment. Data for incidences and multiplicities of pre- and neoplastic liver lesions are summarized in Table 2. Hepatocellular adenomas were observed in 3 *Parp-1*$^{+/+}$ mice given IQ and one each of the *Parp-1*$^{+/-}$ and *Parp-1*$^{-/-}$ mice given IQ, as well as one *Parp-1*$^{+/+}$ mouse maintained on the control diet, and hepatocellular carcinomas (HCC) were seen in one *Parp-1*$^{+/+}$, 2 *Parp-1*$^{+/-}$ and one *Parp-1*$^{-/-}$ mice given IQ, indicating that 300 ppm was not a saturating concentration for tumor induction in the liver. No significant differences were observed in the incidences of these lesions among the *Parp-1* genotypes. Most hepatocellular lesions in *Parp-1*$^{+/+}$ mice were found as single adenomas or adenocarcinomas, but some *Parp-1*$^{+/-}$ and *Parp-1*$^{-/-}$ mice demonstrated more than one tumor. In the lungs, alveolar cell hyperplasias and adenomas were occasionally noted, regardless of the treatment and genotype. Squamous cell hyperplasias of the forestomach ranging from 0.2 to 2.0 mm in diameter were observed more frequently in IQ-treated than in control mice, with no apparent link with the genotype (Table 3).

The relative spleen weights were also significantly higher in *Parp-1*$^{+/+}$ mice given IQ ($P < 0.01$) than in their *Parp-1*$^{+/-}$ and *Parp-1*$^{-/-}$ counterparts. This was associated with a higher incidence of splenomegaly in *Parp-1*$^{+/+}$ (5/17 (29%)) than in *Parp-1*$^{-/-}$ mice (0/19 (0%)), although the difference was not statistically significant (Table 3). Three *Parp-1*$^{+/+}$ mice (18%) and one *Parp-1*$^{-/-}$ mouse (6%) developed malignant lymphomas in the spleen, but the inter-group variation was not significant. In these cases, small foci of atypical lymphocytes were also observed in other organs, such as the liver and kidney.

Table 1
Final body and relative organ weights

Group	Genotype	IQ	No. of mice	Body weight (g)	Relative organ weights (%)		
					Liver	Kidneys	Spleen
1	+/+	+	17	29.2 ± 4.1[a]	6.38 ± 1.59[b]	1.23 ± 0.16[a]	0.65 ± 0.59
2	+/−	+	16	29.4 ± 2.4[a]	5.53 ± 0.68	1.13 ± 0.12[a]	0.32 ± 0.12[d]
3	−/−	+	17	26.5 ± 1.4[a,d,e]	5.93 ± 0.55	1.06 ± 0.08[a,c]	0.28 ± 0.07[d]
4	+/+	−	6	34.8 ± 2.2	4.85 ± 0.59	1.50 ± 0.25	0.31 ± 0.05
5	+/−	−	10	33.4 ± 3.2	5.15 ± 0.85	1.37 ± 0.18	0.43 ± 0.29
6	−/−	−	8	31.8 ± 2.2	5.68 ± 0.43	1.30 ± 0.13	0.39 ± 0.25

[a] Significantly different from control diet group of the same genotype at $P < 0.001$.
[b] Significantly different from control diet group of the same genotype at $P < 0.01$.
[c] Significantly different from +/+ group of the same treatment at $P < 0.001$.
[d] Significantly different from +/+ group of the same treatment at $P < 0.01$.
[e] Significantly different from +/− group of the same treatment at $P < 0.01$.

Table 2
Incidence and multiplicity of liver lesions

Group	Genotype	IQ	No. of mice	Clear cell foci		Hepatocellular carcinoma		Hepatocellular adenoma	
				Incidence (%)	Multiplicity (No./tumor bearing mice)	Incidence (%)	Multiplicity (No./tumor bearing mice)	Incidence (%)	Multiplicity (No./tumor bearing mice)
1	+/+	+	17	1 (6)	2	3 ###	1	1 (6)	1
2	+/−	+	18	1 (6)	1	1 (6)	3	2 ###	2.5±2.1
3	−/−	+	19	0		1 (5)	5	1 (5)	1
4	+/+	−	6	0		1 ###	1	0	
5	+/−	−	10	0		0		0	
6	−/−	−	8	0		0		0	

No brain tumors were noted in our present experiment, unlike the case with *Parp-1*$^{-/-}$ *p53*$^{-/-}$ mice, which have been reported to show a high incidence of brain tumors at week 24 [24].

4. Discussion

The present study demonstrated no increase with *Parp-1* deficiency in the incidences of tumors induced by IQ in the liver, lung and forestomach, which are the main targets for IQ-induced carcinogenesis in mice with the CDF1 genetic background [19]. Although Ohgaki et al. [19] and we used the same dose of IQ (300 ppm in the diet), we observed lower incidences of tumors in the target organs with the present C57BL/6 genetic background. However, the difference could be at least partly explained by the shorter experimental period we applied (60 versus 96 weeks) or a lower susceptibility of C57BL/6 mice to IQ carcinogenicity than with CDF1 mice.

IQ is metabolically activated, mainly in the liver, to form a mutagenic metabolite, *N*-hydroxy-IQ [25], which can be further activated by *O*-acetyl transferase to *N*-acetoxy-IQ [26]. Both *N*-hydroxy-IQ and *N*-acetoxy-IQ covalently bind to DNA, producing *N*-(deoxyguanosin-8-yl)-IQ adducts [27]. Another direct acting mutagen, *N*-nitro-IQ, is also reported to be generated by extrahepatic peroxidases such as prostaglandin H synthase [28]. IQ adducts produced by *N*-hydroxy-IQ, *N*-acetoxy-IQ and *N*-nitro-IQ are suggested to be repaired through nucleotide excision repair (NER) [21], in which Parp-1 is not involved [3]. Therefore, the absence of any difference in susceptibility to IQ-induced carcinogenesis between *Parp-1*$^{-/-}$ and *Parp-1*$^{+/+}$ mice is explainable and provides a sharp contrast to the much elevated susceptibility of *Parp-1*$^{-/-}$ mice on an ICR/129 Sv mixed genetic background to azoxymethane-induced colon and liver tumorigenesis [16], as well as *N*-nitrosobis(2-hydroxypropyl)amine (BHP)-induction of liver hemangiomas and hemangiosarcomas [15]. In BHP-treated mice, we observed a higher frequency of mutations, such as deletions, insertions/rearrangement in *Parp-1*$^{-/-}$ than in *Parp-1*$^{+/+}$ mice [29], providing direct evidence of decreased

Table 3
Incidences of the lesions and abnormality in the lungs, forestomach and spleen (%)

Group	Genotype	IQ	No. of mice	Lungs		Forestomach		Spleen	
				Alveolar cell hyperplasia	Adenoma	Hyperplasia	Papilloma	Splenomegaly	Malignant lymphoma
1	+/+	+	17	2 (12)	0	7 (41)	0	5 (29)	3 (18)
2	+/−	+	18	0	2 (11)	4 (22)	1 (6)	1 (6)	0
3	−/−	+	19	0	0	8 (42)	0	0	1 (6)
4	+/+	−	6	0	0	1 (17)	0	0	0
5	+/−	−	10	0	1 (10)	0	0	3 (30)	2 (20)
6	−/−	−	8	0	0	1 (13)	0	2 (25)	2 (25)

efficiency either in BER or DNA strand break repair. The evidence that Parp-2 is also activated by DNA damages and functions in base excision repair [30] implies the possibility that Parp-2 may complement the activity of Parp-1 in carcinogenesis by IQ. Although it has been suggested that main function of Parp-1 in suppressing the carcinogenesis induced by alkylating agents could not be complemented by Parp-2 or other members of Parp family [15,16], we could not completely exclude this possibility. This point might be further elucidated by studying carcinogenesis induced by IQ in animals with combined Parp-1 and other Parp family member deficiencies.

In line with our results, administration of 4-nitroquinoline 1-oxide (4NQO), which mimics UV induced-DNA damage mainly repaired by NER [31], did not result in a higher incidence of tumors in *Parp-1*$^{-/-}$ than in *Parp-1*$^{+/+}$ mice on an ICR:129/Sv mixed genetic background (Gunji et al., unpublished). Therefore, although the genetic background sometimes affects the outcome of carcinogenesis experiments, in both C57BL/6 and ICR:129/Sv cases, *Parp-1* deficiency did not elevate susceptibility to carcinogenesis induced by carcinogens that generate bulky DNA adducts. Taking all available data together, among the multiple functions of Parp-1, its role in BER and DNA strand break repair is suggested to be most important in the prevention of carcinogenesis. In contrast, *XPA*$^{-/-}$ mice, which lack an important enzyme, XPA, for NER, were found to demonstrate elevated susceptibility to the carcinogenic activity of 2-amino-1-methyl-6-phenylimidazo [4,5-*b*]pyridine (PhIP) [32], another mutagenic and carcinogenic heterocyclic amine, as well as 4NQO-induced oral tumorigenicity [33].

IQ is also reported to induce sister chromatid exchange [34], presumably through non-enzymatic reduction of *N*-nitro-IQ in the presence of NADH and Cu (II) and generation of H_2O_2, which results in oxidative DNA damage [35] in vitro. Free radical generation in the presence of IQ and NADH by recombinant human cytochrome b5 reductase has also been reported [36]. Analysis of mutation frequencies and patterns using Big Blue® rats indicated IQ-DNA adducts rather than IQ-induced oxidative DNA damage to be the major DNA lesions induced by IQ in vivo [37]. The notion that IQ-induced DNA adducts but not IQ-induced oxidative DNA damages are primarily responsible for the IQ-induced carcinogenesis is supported by the present findings. If IQ produces a significant amount of DNA strand breakage or oxidative DNA damage, which is mostly repaired through BER pathway [38], *Parp-1* deficiency would be expected to result in greater tumorigenesis in *Parp-1*$^{-/-}$ than in *Parp-1*$^{+/+}$ mice. The results also provide further evidence that susceptibility to tumorigenesis induced by carcinogens is primarily determined by the efficiency of DNA-repair capacity.

We here noted that, relative liver weights were increased in *Parp-1*$^{+/+}$ mice by IQ treatment ($P < 0.01$), whereas no increase was observed in their *Parp-1*$^{-/-}$ counterparts. Relative spleen weights were also increased in *Parp-1*$^{+/+}$ mice receiving the carcinogen ($P < 0.01$). A defect of S-phase entry in *Parp-1*$^{-/-}$ splenocytes on the C57BL/6 congenic background [39] might be connected with the smaller spleen in *Parp-1*$^{-/-}$ than other genotypes. However, the average relative weight data excluding animals harboring either liver nodules or splenic malignant lymphomas did not show significant differences among the genotypes. Thus, the differences in relative weights might have simply been due to the presence of tumors.

It would be of interest to examine the effect of *Parp-1*-deficiency on IQ-induced carcinogenesis at advanced age after a lower-dose and longer-term treatment with IQ because accumulating studies have indicated that Parp-1 is involved in cell death induction through NAD depletion [4,5]. A role in genome stability could be envisaged through regulation of centrosome function and also cell differentiation.

In conclusion, *Parp-1* deficiency in the present study did not alter the susceptibility to carcinogenesis induced by IQ, which produces bulky DNA adducts that may repaired through NER. This result is in sharp contrast to the elevated susceptibility of *Parp-1*$^{-/-}$ mice to carcinogenesis induced by alkylating agents that produce DNA damage repaired mainly through BER and DNA strand break repair pathways.

Acknowledgements

This work was supported in part by Grants-Aid for Cancer Research from the Ministry of Education, Culture, Sports, Science and Technology, and the Ministry of Health, Labour and Welfare, a Grant-in-aid from the Ministry of Health, Labour and Welfare for the Second and Third Term Comprehensive 10-Year Strategy for Cancer Control, Japan, and a grant from the Society for Promotion of Toxicological Pathology of Nagoya, Japan.

References

[1] M. Nakayasu, H. Shima, S. Aonuma, H. Nakagama, M. Nagao, T. Sugimura, Deletion of transfected oncogenes from NIH 3T3 transformants by inhibitors of poly(ADP-ribose) polymerase, Proc. Natl Acad. Sci. USA 85 (1988) 9066–9070.

[2] B.W. Durkacz, O. Omidiji, D.A. Gray, S. Shall, (ADP-ribose) n participates in DNA excision repair, Nature 283 (1980) 593–596.

[3] Z.Q. Wang, L. Stingl, C. Morrison, M. Jantsch, M. Los, K. Schulze-Osthoff, et al., PARP is important for genomic stability but dispensable in apoptosis, Genes Dev. 11 (1997) 2347–2358.

[4] H. Yamamoto, H. Okamoto, Protection by picolinamide, a novel inhibitor of poly (ADP-ribose) synthetase, against both streptozotocin-induced depression of proinsulin synthesis and reduction of NAD content in pancreatic islets, Biochem. Biophys. Res. Commun. 95 (1980) 474–481.

[5] S.W. Yu, H. Wang, M.F. Poitras, C. Coombs, W.J. Bowers, H.J. Federoff, et al., Mediation of poly(ADP-ribose) polymerase-1-dependent cell death by apoptosis-inducing factor, Science 297 (2002) 259–263.

[6] Y. Ohashi, K. Ueda, O. Hayaishi, K. Ikai, O. Niwa, Induction of murine teratocarcinoma cell differentiation by suppression of poly(ADP-ribose) synthesis, Proc. Natl Acad. Sci. USA 81 (1984) 7132–7136.

[7] M.E. Smulson, V.H. Kang, J.M. Ntambi, D.S. Rosenthal, R. Ding, C.M. Simbulan, Requirement for the expression of poly(ADP-ribose) polymerase during the early stages of differentiation of 3T3-L1 preadipocytes, as studied by antisense RNA induction, J. Biol. Chem. 270 (1995) 119–127.

[8] M. Hemberger, T. Nozaki, E. Winterhager, H. Yamamoto, H. Nakagama, N. Kamada, et al., *Parp1*-deficiency induces differentiation of ES cells into trophoblast derivatives, Dev. Biol. 257 (2003) 371–381.

[9] M. Masutani, H. Nakagama, T. Sugimura, Poly(ADP-ribose) and carcinogenesis, Gen. Chrom. Cancer 38 (2003) 339–348.

[10] C. Bernstein, H. Bernstein, C.M. Payne, H. Garewal, DNA repair/pro-apoptotic dual-role proteins in five major DNA repair pathways: fail-safe protection against carcinogenesis, Mutat. Res. 511 (2002) 145–178.

[11] F. Dantzer, V. Schreiber, C. Niedergang, C. Trucco, E. Flatter, G. De La Rubia, et al., Involvement of poly(ADP-ribose) polymerase in base excision repair, Biochimie 81 (1999) 69–75.

[12] V. Rolli, A. Ruf, A. Augustin, G.E. Schulz, J. Menissier-de, G. de Murcia, Poly(ADP-ribose) polymerase: structure and function in: G. de Murcia, S. Shall (Eds.), From DNA damage and stress signaling to cell death: poly ADP-ribosylation reactions, Oxford University Press, New York, 2000, pp. 35–79.

[13] Y.G. Yang, U. Cortes, S. Patnaik, M. Jasin, Z.Q. Wang, Ablation of PARP-1 does not interfere with the repair of DNA double-strand breaks, but compromises the reactivation of stalled replication forks, Oncogene 23 (2004) 3872–3882.

[14] M. Masutani, H. Suzuki, N. Kamada, M. Watanabe, O. Ueda, T. Nozaki, et al., Poly(ADP-ribose) polymerase gene disruption conferred mice resistant to streptozotocin-induced diabetes, Proc. Natl Acad. Sci. USA 96 (1999) 2301–2304.

[15] M. Tsutsumi, M. Masutani, T. Nozaki, O. Kusuoka, T. Tsujiuchi, H. Nakagama, et al., Increased susceptibility of poly(ADP-ribose) polymerase-1 knockout mice to nitrosamine carcinogenicity, Carcinogenesis 22 (2001) 1–3.

[16] T. Nozaki, H. Fujihara, M. Watanabe, M. Tsutsumi, K. Nakamoto, O. Kusuoka, et al., *Parp-1* deficiency implicated in colon and liver tumorigenesis induced by azoxymethane, Cancer Sci. 94 (2003) 497–500.

[17] W.M. Tong, U. Cortes, M.P. Hande, H. Ohgaki, L.R. Cavalli, P.M. Lansdorp, et al., Synergistic role of Ku80 and poly(ADP-ribose) polymerase in suppressing chromosomal aberrations and liver cancer formation, Cancer Res. 62 (2002) 6990–6996.

[18] M. Masutani, A. Gunji, M. Tsutsumi, K. Ogawa, N. Kamada, T. Shirai, et al., Role of poly-ADP-ribosylation in cancer development, in: A. Buerkle (Eds.), Poly(ADP-ribosyl)ation, Landes Bioscience/Eurekah.com, Georgetown, in press.

[19] H. Ohgaki, K. Kusama, N. Matsukura, K. Morino, H. Hasegawa, S. Sato, et al., Carcinogenicity in mice of a mutagenic compound, 2-amino-3-methylimidazo[4,5-f]quioline, from broiled sardine, cooked bee and beef extract, carcinogenesis 5 (1984) 921–924.

[20] T. Sugimura, Studies on environmental chemical carcinogenesis in Japan, Science 233 (1986) 312–318.

[21] R.W. Wu, F.N. Panteleakos, J.S. Felton, Development and characterization of CHO repair-proficient cell lines for comparative mutagenicity and metabolism of heterocyclic amines from cooked food, Environ. Mol. Mutagen 41 (2003) 7–13.

[22] R.W. Sobol, D.E. Watson, J. Nakamura, F.M. Yakes, E. Hou, J.K. Horton, et al., Mutations associated with base excision repair deficiency and methylation-induced genotoxic stress, Proc natl Acad Sci USA 99 (2002) 6860–6865.

[23] F. tanabe, H. Fukazawa, M. Masutani, H. Suzuki, H. Teraoka, S. Mizutani, et al., Poly(ADP-ribose) polymerase-1 inhibits ATM kinase activity in DNA damage response, Biochem. Biophys. Res. Commun. 319 (2004) 596–602.

[24] W.M. Tong, H. Ohgaki, H. Huang, C. Granier, P. Kleihues, Z.Q. Wang, Null mutation of DNA strand break-binding molecule poly(ADP-ribose) polymerase causes medulloblastomas in *p53*(−/−) mice, Am. J. Pathol. 162 (2003) 343–352.

[25] T. Okamoto, K. Shudo, Y. Hashimoto, T. Kosuge, T. Sugimura, S. Nishimura, Identification of a reactive metabolite of the mutagen, 2-amino-3-methylimidazolo[4,5-*f*]quinoline, Chem. Pharm. Bull. (Tokyo) 29 (1981) 590–593.

[26] E.G. Snyderwine, P.J. Wirth, P.P. Roller, R.H. Adamson, S. Sato, S.S. Thorgeirsson, Mutagenicity and in vitro covalent DNA binding of 2-hydroxyamino-3-methylimidazolo[4,5-*f*] quinoline, Carcinogenesis 9 (1988) 411–418.

[27] E.G. Snyderwine, P.P. Roller, R.H. Adamson, S. Sato, S.S. Thorgeirsson, Reaction of *N*-hydroxylamine and *N*-acetoxy derivatives of 2-amino-3-methylimidazolo[4,5-*f*] quinoline with DNA. Synthesis and identification of *N*-(deoxyguanosin-8-yl)-IQ, Carcinogenesis 9 (1988) 1061–1065.

[28] L.D. Morrison, T.E. Eling, P.D. Josephy, Prostaglandin H synthase-dependent formation of the direct-acting mutagen 2-nitro-3-methylimidazo[4,5-*f*]quinoline (nitro-IQ) from IQ, Mutat. Res. 302 (1993) 45–52.

[29] A. Shibata, N. Kamada, K.-i. Masumura, T. Nohmi, S. Kobayashi, H. Teraoka, et al., *Parp-1* deficiency causes an increase of deletion mutations and insertions/rearrangements *in vivo* after treatment with an alkylating agent, Oncogene 24 (2005) 1328–1337.

[30] V. Schreiber, J.C. Ame, P. Dolle, I. Schultz, B. Rinaldi, V. Fraulob, et al., Poly(ADP-ribose) polymerase-2 (PARP-2) is required for efficient base excision DNA repair in association with PARP-1 and XRCC1, J. Biol. Chem. 277 (2002) 23028–23036.

[31] S. Kondo, A test for mutation theory of cancer: carcinogenesis by misrepair of DNA damaged by 4-nitroquinoline 1-oxide, Br. J. Cancer 35 (1977) 595–601.

[32] J.C. Klein, R.B. Beems, P.E. Zwart, M. Hamzink, G. Zomer, H. van Steeg, et al., Intestinal toxicity and carcinogenic potential of the food mutagen 2-amino-1-methyl-6-phenylimidazo[4,5-b]pyridine (PhIP) in DNA repair deficient XPA−/− mice, Carcinogenesis 22 (2001) 619–626.

[33] F. Ide, H. Oda, Y. Nakatsuru, K. Kusama, H. Sakashita, K. Tanaka, et al., Xeroderma pigmentosum group A gene action as a protection factor against 4-nitroquinoline 1-oxide-induced tongue carcinogenesis, Carcinogenesis 22 (2001) 567–572.

[34] L.H. Thompson, A.V. Carrano, E. Salazar, J.S. Felton, F.T. Hatch, Comparative genotoxic effects of the cooked-food-related mutagens Trp-P-2 and IQ in bacteria and cultured mammalian cells, Mutat. Res. 117 (1983) 243–257.

[35] M. Murata, M. Kobayashi, S. Kawanishi, Nonenzymatic reduction of nitro derivative of a heterocyclic amine IQ by NADH and Cu(II) leads to oxidative DNA damage, Biochemistry 38 (1999) 7624–7629.

[36] H. Maeda, T. Sawa, T. Yubisui, T. Akaike, Free radical generation from heterocyclic amines by cytochrome b5 reductase in the presence of NADH, Cancer Lett. 143 (1999) 117–121.

[37] P. Møller, H. Wallin, U. Vogel, H. Autrup, L. Risom, M.T. Hald, et al., Mutagenicity of 2-amino-3-methylimidazo[4,5-*f*]quinoline in colon and liver of Big Blue rats: role of DNA adducts, strand breaks, DNA repair and oxidative stress, Carcinogenesis 23 (2002) 1379–1385.

[38] P.M. Girard, S. Boiteux, Repair of oxidized DNA bases in the yeast *Saccharomyces cerevisiae*, Biochimie 79 (1997) 559–566.

[39] F. Watanabe, M. Masutani, N. Kamada, H. Suzuki, H. Nakagama, T. Sugimura, et al., Impairment in S-phase entry of splenocytes of *Parp-1* knockout mice, Proc. Jpn Acad. 79 Ser. B (2003) 248–251.

Available online at www.sciencedirect.com
SCIENCE DIRECT
ELSEVIER
Mutation Research 598 (2006) 120–131
Fundamental and Molecular Mechanisms of Mutagenesis
www.elsevier.com/locate/molmut
Community address: www.elsevier.com/locate/mutres

Molecular mechanisms for maintenance of G-rich short tandem repeats capable of adopting G4 DNA structures

Hitoshi Nakagama*, Kumiko Higuchi, Etsuko Tanaka, Naoto Tsuchiya, Katsuhiko Nakashima, Masato Katahira, Hirokazu Fukuda

Biochemistry Division, National Cancer Center Research Institute, 5-1-1 Tsukiji, Chuo-ku, Tokyo 104-0045, Japan

Available online 2 March 2006

Abstract

Mammalian genomes contain several types of repetitive sequences. Some of these sequences are implicated in various specific cellular events, including meiotic recombination, chromosomal breaks and transcriptional regulation, and also in several human disorders. In this review, we document the formation of DNA secondary structures by the G-rich repetitive sequences that have been found in several minisatellites, telomeres and in various triplet repeats, and report their effects on in vitro DNA synthesis. d(GGCAG) repeats in the mouse minisatellite Pc-1 were demonstrated to form an intra-molecular folded-back quadruplex structure (also called a G4′ structure) by NMR and CD spectrum analyses. d(TTAGGG) telomere repeats and d(CGG) triplet repeats were also shown to form G4′ and other unspecified higher order structures, respectively. In vitro DNA synthesis was substantially arrested within the repeats, and this could be responsible for the preferential mutability of the G-rich repetitive sequences. Electrophoretic mobility shift assays using NIH3T3 cell extracts revealed heterogeneous nuclear ribonucleoprotein (hnRNP) A1 and A3, which were tightly and specifically bound to d(GGCAG) and d(TTAGGG) repeats with K_d values in the order of nM. HnRNP A1 unfolded the G4′ structure formed in the $d(GGCAG)_n$ and $d(TTAGGG)_n$ repeat regions, and also resolved the higher order structure formed by d(CGG) triplet repeats. Furthermore, DNA synthesis arrest at the secondary structures of d(GGCAG) repeats, telomeres and d(CGG) triplet repeats was efficiently repressed by the addition of hnRNP A1. High expression of hnRNPs may contribute to the maintenance of G-rich repetitive sequences, including telomere repeats, and may also participate in ensuring the stability of the genome in cells with enhanced proliferation. Transcriptional regulation of genes, such as *c-myc* and *insulin*, by G4 sequences found in the promoter regions could be an intriguing field of research and help further elucidate the biological functions of the hnRNP family of proteins in human diseases.

Keywords: Molecular mechanism; G4 DNA structure; G-rich repetitive sequence; hnRNPs

1. Introduction

Mammalian genomes are known to contain various types of repetitive sequences, including microsatellites, triplet repeats, minisatellites, and telomeres [1]. LINE, SINE and LTR sequences are also frequently found in the genome of vertebrates [2]. Although there is some variation in the size definition for repeat families, microsatellite repeats are generally composed of short repetitive units of less than 6 nucleotides [1]. It is estimated that more than 100,000 microsatellite loci occur in the mammalian genome. Microsatellites are typically less than 100 base pairs (bp) in total length [3]. Although triplet repeats are also categorized as members of the microsatellite family, some triplet repeat loci can

* Corresponding author. Tel.: +81 3 3547 5239; fax: +81 3 3542 2530.
E-mail address: hnakagam@gan2.res.ncc.go.jp (H. Nakagama).

0027-5107/$ – see front matter © 2006 Elsevier B.V. All rights reserved.
doi:10.1016/j.mrfmmm.2006.01.014

expand to hundreds or even thousands of repeats in certain human disorders (e.g., fragile X syndrome, myotonic dystrophy, Huntington disease) by un-clarified mechanisms [4,5]. In contrast, minisatellite repeats (also known as variable number of tandem repeats; VNTR) are composed of longer repetitive units of 5 or 6–100 nucleotides and are found in arrays expanded up to 10–20 kbp. As opposed to microsatellites, only a few 1000 such loci are present in the genome [6]. Although the biological significance of minisatellite repeats remains largely unknown, some repeat regions are known to be hotspots for meiotic recombination [7,8]. They are also occasionally found in fragile chromosomal sites and could serve as targets for genomic recombination or chromosomal breakage [9,10].

Genetic alteration at a few specific microsatellite and minisatellite repeats results in several human disorders. Alterations in microsatellite repeats are frequently found in cancer cells, and are caused by both genetic and functional alterations of genes encoding mismatch repair proteins, including MLH1, MSH2, MSH6, PMS1, PMS2 and MLH3 [11,12]. Mutations in mismatch repair genes, as occurs in hereditary non-polyposis colorectal cancers, lead to microsatellite instabililty (MSI). MSI can, in turn, cause frame-shift mutations in long tracts of mononucleotides; examples of this have been observed in the transforming growth factor-β type II, BAX and insulin-like growth factor II receptor genes [11,12]. Under mismatch repair-deficient conditions, microsatellite repeats are altered by the insertion or deletion of small numbers of mono- or di-nucleotide repeat units [11,12].

Alteration at certain minisatelllite loci are also implicated in genetic predisposition to some human disorders, such as insulin-dependent diabetes mellitus type 2 (IDDM-2) [13]. A rare allele of the Ha-*ras*-VNTR, which is located in the 3′ region of the Ha-*ras* gene, appears to be associated with various cancers including breast, colon, urinary bladder and acute leukemia [14].

In this review article, characteristic structural features of G-rich short tandem repeats are summarized, and molecular mechanisms involved in maintaining genomic stability at these G-rich repetitive sequences are discussed.

2. Minisatellite Pc-1 and Pc-1-like repeats

The mouse Pc-1 minisatellite (also known as the expanded simple tandem repeat *Ms6-hm*) consists of a tandem array of G-rich repeats $d(GGCAG)_n$, flanked with locus specific sequence [15]. The length of the repeat arrays vary widely among mouse strains [16,17]. Pc-1 was observed to be a recombination hotspot at meiosis, with a germ-line mutation rate as high as 10% per gamete [18,19]. In normal somatic cells, however, the repeats are relatively stable and the mutation rate has been estimated to be around 2×10^{-9} per cell division [17]. To date, many hypervariable minisatellites, consisting of G-rich repeat units similar to Pc-1, have been identified in the mouse and other mammalian genomes. Mouse loci Pc-2 and mo-1 are composed of d(GGCAGG) and d(CTGGGCAGGGAGGA) repeats [16], and human 33.6 and 33.15 minisatellites consist of d(AGGGCTGGAGG) and d(AGAGGTGGGCAGGTGG) repeats, respectively [20]. Since the core sequences of G-rich minisatellites share high similarity among the repeats, more than 20–30 bands are easily detected in mouse and human genomes by a low-stringent DNA fingerprint analysis using Pc-1 as a probe [21,22]. These Pc-1-like repeats are also stable in normal somatic cells, although there are several conditions that can induce mutational instability at this locus [19,21–23].

3. Size alteration of G-rich minisatellite repeats in the genome

Minisatellite repeats are generally stable in somatic cells compared to germ cells as described above [24–26], but alterations at minisatellite regions can be induced both in cell cultures and in vivo [21,27–31]. When culture cells are exposed to a variety of chemical carcinogens, ultraviolet irradiation or ionizing radiation, DNA fingerprint analysis reveals alterations of the banding pattern of genomic regions containing tandem repeats. We hereafter refer to these genetic alterations in minisatellite regions as 'minisatellite mutations', which may include, for example, changes in non-repeat flanking regions and restriction endonuclease sites, deletions/insertions within the repeat regions, and recombination events. Additionally, these types of mutations are frequently observed in sporadic human colorectal and gastric cancers, the incidence being 56% and 25%, respectively [22].

Minisatellite instability is an interesting phenomenon that is suggestive of a novel type of genomic instability [9,23]. As we reported previously, minisatellite instability was observed in a Scid fibroblast cell line transformed by simian virus 40 (SV40) large tumor antigen, SC3VA2, and an embryonal Scid fibroblast cell line, SC1K [23]. Both of these cell lines are deficient in DNA-dependent protein kinase (DNA-PK) activity. A considerable number of size alterations in minisatellites were observed in subclones of both the SC3VA2 and

SC1K cells (45 ± 6% and 37 ± 3%, respectively). These findings were corroborated in several sets of clones. In contrast, cells derived from the RD13B2 cell line, which was established from SC3VA2 by introducing a fragment of the human chromosome 8q, which includes the DNA-PK catalytic subunit, showed a very low frequency of minisatellite mutation (3 ± 3%). Although the underlying molecular mechanisms for this instability have not yet been fully elucidated, a lack of correlation between the presence of minisatellite mutations and microsatellite mutation/instability [21–23] suggests that the mismatch repair system is not involved. Therefore, it appears that another, as yet undiscovered mechanism specific to minisatellite instability, is at play in this case.

4. Formation of G4′ structure by d(GGCAG)$_n$ in vitro

We used structural analyses to investigate whether higher order structures occur in G-rich repetitive sequences to gain further insight into the molecular mechanisms operating in induced instability at these sites. The formation of secondary structures is likely due to the G-rich nature of the repeats. For example, a triple-stranded DNA between d(GGA:TCC) repeats and d(GGA) repeat oligonucleotides forms a D-loop-like higher order structure [32]. The d(CTG:CAG) repeats from the myotonic dystrophy locus form slipped-strand DNA (S-DNA) [33]. A polymorphic G-rich minisatellite, d(ACAGGGGTGTGGGG)$_n$, located in the promoter region of the human insulin gene [34], the G-rich immunoglobulin switch repeats [35], and the G-rich sequence d(G$_{16}$CG(GGT)$_2$GG) in the promoter region of the chicken β-globin gene are also known to form unusual DNA structures, such as four-stranded quadruplexes [36].

Based on these observations, genomic instability at G-rich minisatellites may also be caused as a consequence of the formation of higher order structures of DNA. To investigate this hypothesis, we used the Pc-1 minisatellite repeat, d(GGCAG), as a representative G-rich minisatellite locus of the mouse genome. As shown in Fig. 1A, NMR analysis demonstrated that a synthetic oligonucleotide containing eight repeats of d(GGCAG) (d(GGCAG)$_8$) has the characteristic features necessary to form a quadruplex structure [37]. Circular dichroism (CD) spectrum analysis showed a specific positive CD band at 290–295 nm (Fig. 1B). A positive peak at 260 nm, which is characteristic of the quadruplex with a four-stranded (inter-strand) parallel quadruplex as detailed previously [34,38], was not observed. Furthermore, melting temperatures of oligonucleotides d(GGCAG)$_8$ and d(GGCAG)$_5$ determined by thermal CD melting curves under physiological conditions (100 mM KCl) were independent of DNA concentration. As a reference, a 10-fold dilution of DNA concentration for duplexed DNA causes a 6–8 °C drop of the melting temperature [39]. Taken together, the data indicate that d(GGCAG)$_8$ and d(GGCAG)$_5$ form intra-strand folded-back quadruplex structures (also called a G4′-structure) as opposed to four-stranded quadruplex structures (G4-structure) [37]. The CD spectrum of d(GGCAG)$_3$ was different from those of d(GGCAG)$_5$ and d(GGCAG)$_8$, and gave a broad positive band around 280 nm, but not the typical positive band of the G4′ structure at 290–295 nm (data not shown). Taken together, intra-molecular G:G:G:G tetrad formation with four d(GGG) sequences in d(GGCAG)$_n$

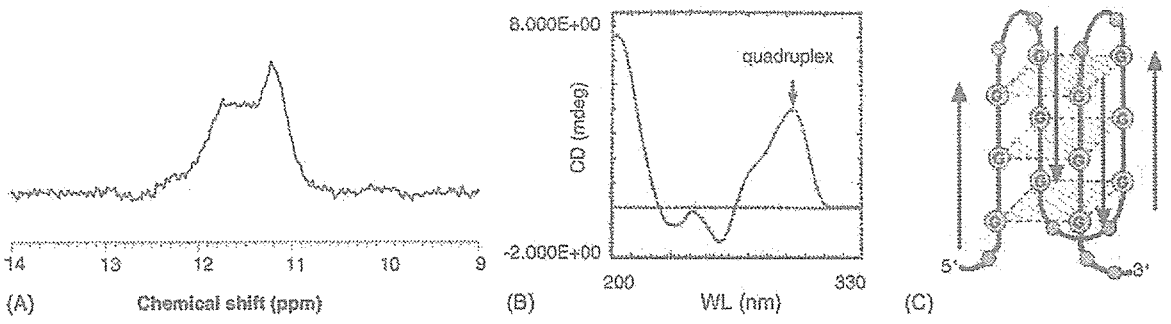

Fig. 1. NMR and CD analysis of d(GGCAG)$_8$ (A) Imino proton NMR spectrum of d(GGCAG)$_8$ in ^2H_2O. The appearance of signals around at 11–12 ppm even in ^2H_2O at 5 °C is characteristic of a quadruplex structure with guanine-quartets. (B) A positive CD band at 290–295 nm is characteristic of a quadruplex with a folded-back structure. A four-stranded parallel quadruplex does not give a positive band at 290–295 nm, but gives one at 260 nm. (C) Schematic diagram illustrating how the d(GGCAG) repeats form a G4′ structure is depicted, although we have not determined yet whether the G4′ structure formed by d(GGCAG) repeats is a "chair" or "basket" type quadruplex [79]. In this model, one G-stretch is aligned anti-parallel to the next G-stretch, and four guanine residues are arranged in a square-planar array.

repeats ($n \geq 5$) could explain the formation of a G4′ structure, as depicted in Fig. 1C.

Although we have not yet proven the in vivo formation of a G4′ structure by d(GGCAG) minisatellite repeats, recent studies by Duquette et al. [40] and Paeschke et al. [41] strongly support the formation of G-quadruplex DNA structures in vivo. Duquette et al. demonstrated the formation of G-loops, novel structures containing G4 DNA, in *E. coli* using plasmid harboring the G-rich regions derived from the mammalian immunoglobulin S (switch) regions and GQN1, an endonuclease that specifically cleaves G4 DNA in the single stranded region 5′ of the stacked G-quartet [42]. Paeschke et al. beautifully demonstrated G-quadruplex formation in the macronucleus of the ciliated *Stylonychia* [41] by the use of antibodies specific for telomeric G-quadruplex DNA [43]. These findings support the hypothesis that G4′ DNA structures form at Pc-1 and Pc-1-like minisatellite repeats in vivo as well. However, further studies are required to validate this hypothesis.

5. DNA synthesis arrest at the d(GGG) sites in vitro

Several studies have demonstrated the ability of d(GGG) sites to cause DNA synthesis arrest. For example, the in vitro DNA synthesis assay showed DNA synthesis arrest at the first d(GGG) site of a single-stranded phagemid (pYA-3) carrying 12 repeats of d(GGCAG), with additional weaker stops at the second, third and fourth d(GGG) sequences (Fig. 2). A primer extension reaction using a synthetic oligonucleotide containing $d(GGCAG)_{15}$ gave similar results (further described below). Inhibition of in vitro DNA synthesis by the formation of G-quadruplex was also reported previously using synthetic oligonucleotides of human $[d(TTAGGG)_n]$, the *Tetrahymena* $[d(TTGGGG)_n]$ telomeric sequences [44] and the G-rich sequence found in the promoter region of the chicken β-globin gene, $d(G_{16}CG(GGT)_2GG)$ [36,45].

Recently, we found that DNA replication of plasmid in *E. coli* was substantially affected by the presence of d(GGCAG) repeats (unpublished observations). Considering both in vitro and in vivo data, it appears that the presence of the G-rich repeats in the template may inhibit normal DNA synthesis (replication). If this is the case, the lack of repeat instability in somatic cells suggests that somatic cells may have specialized machinery to compensate for the formation of unfavourable higher order DNA structures and to allow replication through the G-rich repeats.

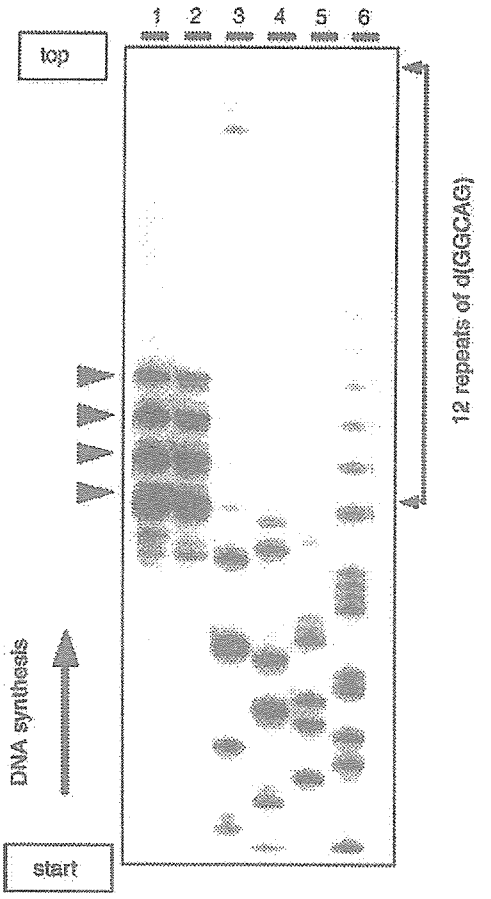

Fig. 2. In vitro DNA synthesis assay using a single-stranded phagemid carrying a $d(GGCAG)_{12}$ repeat. Primer extension reaction was performed as follows using the single-stranded phagemid pYA-3 carrying $d(GGCAG)_{12}$ [37]. The pUC/M13-M4 forward primer (Takara) labeled with ^{32}P at the 5′-end (600 fmol) was annealed with single-stranded pYA-3 (250 fmol) in 5 μl of buffer (40 mM Tris–HCl pH 7.5, 20 mM $MgCl_2$, 50 mM KCl, 5 μM dNTPs) at 72 °C for 5 min, followed by slow cooling to 37 °C. The reaction was started by the addition of 0.5 μl of Sequenase (0.8 U) or the Klenow Fragment (1.0 U), and the mixture was further incubated at 37 °C for 10 min. The reaction was stopped by adding 3.5 μl of the stop solution (10 mM NaOH, 95% formamide, 0.05% bromophenol blue, 0.05% xylene cyanole) and after incubation at 95 °C for 2 min, 3 μl aliquots of the sample DNA were electrophoresed in an 8% polyacrylamide gel containing 7 M urea. Polyacrylamide gel electrophoresis (PAGE) analysis of primer extension reaction with Sequenase (lane 1) or Klenow (lane 2) clearly shows the arrest of in vitro DNA synthesis at the first to fourth d(GGG) sites (arrow heads). Lanes 3–6 show the sequencing reactions with Sequenase in the presence of ddATP, ddTTP, ddCTP and ddGTP, respectively, using 200 fmol of single-stranded pYA-3 plasmids for each reaction. An arrow at the left indicates the direction of DNA synthesis.

6. Isolation of G-rich minisatellite binding proteins

To elucidate the underlying molecular mechanisms for maintenance of genomic stability at genomic G-

Table 1
Isolation of minisatellite binding proteins from NIH3T3 cell extract [48]

ID	MW (kDa)	Common name
MNBP-A	30	hnRNP A3
MNBP-B	24	hnRNP A1/UP1
MNBP-D	29	ND[a]
MNBP-E	98	LRP130[b]
MNBP-F	130	LRP130
MNBP-G	110	Tudor-SN/SND1

[a] ND: not determined.
[b] Probably a proteolytic product of MNBP-F, LRP130.

Table 2
IC_{50} values for formation of d(GGCAG)$_8$–protein complexes with hnRNP A1, hnRNP A3 and UP1 [48,52]

Competitor	hnRNP A1	hnRNP A3	UP1
$G5_{TEL}$ ((GTTAGG)$_5$)	3 nM	5 nM	3 nM
$G5_{+T}$ ((GTCAGG)$_5$)	1 nM	7 nM	4 nM
$G5_{Pc\text{-}2}$ ((GGCAGG)$_5$)	9 nM	20 nM	40 nM
G5 ((GGCAG)$_5$)	6 nM	300 nM	20 nM
Poly(dG) ((dG)$_{25}$)	9 nM	1 μM	100 nM
$G5_{+C}$ ((GCCAGG)$_5$)	>1 μM	>1 μM	>1 μM

IC_{50} values were estimated from the inhibition curves generated by plotting the relative amount of complex against the concentration of a competitor, and expressed as the concentrations of individual unlabeled competitor oligonucletides at which the labeled d(GGCAG)$_8$–protein complex yield was halved. The concentration of labeled d(GGCAG)$_8$ used in the competition reaction is 2 nM in all experiments.

rich minisatellite sequences, we carried out an electrophoretic mobility shift assay (EMSA) to identify minisatellite binding proteins (MNBPs) using cell-free extracts from NIH3T3 cells treated with okadaic acid (Table 1). Okadaic acid (OA) is a known tumor promoter [46] and a specific inhibitor of the mammalian serine/threonine protein phosphatases [47]. OA is capable of inducing minisatellite mutations in NIH3T3 cells [21]. Two proteins, hnRNP A3 (MNBP-A) and hnRNP A1 (MNBP-B), were identified from OA-treated NIH3T3 cells as MNBPs for the G-rich strand of the Pc-1 minisatellite [48]. In addition, three proteins, MNBP-D, LRP130 (MNBP-E and -F) and Tudor-SN/SND1 (MNBP-G), were identified as C-rich strand binding proteins [48], whose functions and biological consequences will be briefly discussed later.

Binding of hnRNP A1 in cell-free extracts to the G-rich repeat was enhanced from cultures treated with 5 nM of OA. In contrast, hnRNP A3 did not show any such enhancement after OA treatment, suggesting some mechanistic differences in DNA recognition and binding between the two hnRNPs. Sequence requirements for the high-binding affinity of hnRNP A1 and hnRNP A3 were evaluated by an oligonucleotide competition assay using EMSA, and are summarized in Table 2. hnRNP A1 binds more widely to d(GGCAG)$_5$ and d(GGCAG)-like repeats, including $G5_{TEL}$, $G5_{+T}$ and poly(dG), with a K_d value of nM magnitudes. Interestingly, the affinity of hnRNA3 with d(GGCAG)$_5$ was about 50-fold weaker than that of hnRNP A1, with IC_{50} values for the formation of d(GGCAG)$_8$-protein complexes being 300 and 6 nM, respectively (see footnote for Table 2). This suggests that tandem arrays ($n>5$ units) are required for sufficient binding of hnRNP A3 with Pc-1 d(GGCAG)$_n$ repeats. In contrast, competition with telomere repeats ($G5_{TEL}$) and telomere-like repeats ($G5_{+T}$) showed much stronger inhibitory activity for hnRNP A3 binding to d(GGCAG)$_8$, the value of which was almost comparable to that observed for hnRNP A1. $G5_{Pc\text{-}2}$, which contains a G-insertion in the d(GGCAG) repeat of Pc-1, and is similar to minisatellite Pc-2, showed a slightly lower binding activity than the d(GGCAG) repeats. $G5_{+C}$ did not bind to either hnRNP A1 or hnRNP A3. A large difference was also observed between hnRNP A1 and hnRNP A3 with poly (dG) probes. Binding of hnRNP A3 to poly(dG) was 100-fold weaker than hnRNP A1.

Based on our data, minisatellite Pc-1 binding proteins are able to bind not only to Pc-1 but also to other minisatellites having Pc-1-like sequences. Sequence requirements for DNA binding of hnRNP A3 seem to be stricter than those for hnRNP A1, and this suggests that hnRNP A3 may serve a different function from hnRNP A1 by binding to separate regions of the genome. Both hnRNP A1 and hnRNP A3 may be telomere binding proteins, and elucidation of the biological functions of hnRNP A3 is currently ongoing in our laboratory.

7. hnRNP A1 and UP1 bind to G-rich repetitive sequences and unfold G4′ structures

To clarify the consequence of hnRNP A1 binding to G-rich repetitive sequences, we investigated its effect on the stability of the G4′ structure. Recombinant hnRNP A1 and unwinding protein 1 (UP1), a proteolytic product of hnRNP A1 lacking the C-terminal portion of hnRNP A1 [49–51], were expressed in *E. coli* as GST fusion proteins and purified, by releasing a GST tag, for use in G4′ binding assays. DNA binding affinity and sequence specificity of UP1 is almost equivalent to those of GST-UP1 and GST-hnRNP A1, but is slightly lower than that of hnRNP A1 (Table 2).

By EMSA, the intramolecular quadruplex (G4′ form) of d(GGCAG)$_8$ shows faster mobility than the single-stranded form on polyacrylamide gel electrophoresis (PAGE). Both UP1 and GST-hnRNP A1 bind to both

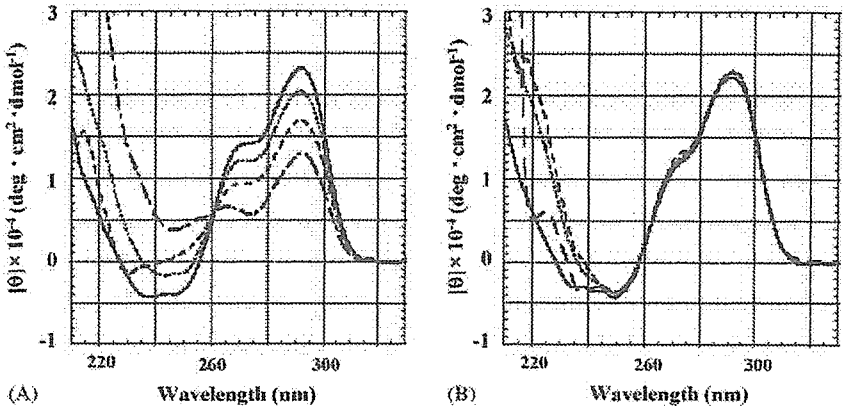

Fig. 3. CD spectra indicate UP1 unfolds the G4′ structure of d(GGCAG) repeats. CD spectra of $d(GGCAG)_5$ with GST-UP1 (A) and GST (B). For each CD spectrum, the spectrum of the corresponding protein was subtracted. Solid, the DNA:protein molar ratio of 1:0; dotted, 1:0.5; dashed, 1:1; centered, 1:2. The CD band at 290–295 nm was decreased by addition of GST-UP1 in a dose-dependent manner. GST alone did not induce any change in the levels of the peak.

G4′ and single-stranded forms of $d(GGCAG)_8$ [52], and decrease, in a dose dependent manner, the amount of the G4′ form (unpublished data). The characteristic CD band at 290–295 nm of the G4′ structure was decreased by addition of GST-UP1 in a concentration-dependent manner (Fig. 3A), while the addition of GST did not induce any change (Fig. 3B). These data clearly indicate that hnRNP A1 and UP1 unfold the G4′ structure at the d(GGCAG) repeats.

Another member of the hnRNP family proteins, hnRNP D, also binds and destabilizes the quadruplex structure formed by telomeric $d(TTAGGG)_n$ repeats, and is suggested to be involved in maintenance of the telomere 3′-overhang [53]. LR1, a heterodimer of nucleolin and hnRNP D, binds to duplex DNA sites in the immunoglobulin heavy chain switch (S) regions, which are G-rich DNA regions conforming to the consensus sequence, dGGNCNAG(G/C)CTG(G/A) [54]. Dempsey et al. demonstrated LR1 binding to G4 DNA formed by G-G pairing in S region sequences, and suggested that LR1 may juxtapose donor and acceptor switch regions for recombination during S region transcription [54]. Two hnRNP-related telomeric DNA-binding proteins, uqTBP25 and qTBP42, which show close sequence similarity to hnRNP A1, hnRNP A2/B1 and/or hnRNP C, also bind to quadruplex telomeric DNA and increase the heat stability and resistance of the telomeric repeats to micrococcal nuclease digestion [55,56]. Weisman-Shomer et al. recently demonstrated that both uqTBP25 and qTBP42 destabilize the quadruplex (tetraplex) structures of $d(CGG)_n$, but quadruplex structures of telomeric and IgG sequences are resistant to destabilization by these two proteins, suggesting the presence of some structural differences among the quadruplexes [57].

8. Abrogation of DNA synthesis arrest at the G4′ structure by UP1

When template carrying $d(GGCAG)_{12}$ was used for an in vitro DNA synthesis assay, a primer extension reaction with *BcaBEST* DNA polymerase was obstructed mainly at the first d(GGG) site (Fig. 4A). A primer extension reaction with a synthetic oligonucleotide containing a $d(CAGGG)_{15}$ repeat also demonstrated that progression of DNA polymerase was obstructed mainly at the first d(GGG) site followed by additional weaker stops at the second, third, fourth, fifth and sixth d(GGG) sites (Fig. 4B). When UP1 was added to the reaction with an excess molar amount over the template, DNA synthesis arrest at the d(GGG) sites was reduced in a dose-dependent manner and the synthesis of the complete length of template DNA was considerably enhanced (Fig. 4A and B). Other DNA polymerases, such as Taq, Klenow fragment and human DNA polymerase α (pol α) also gave similar results [52]. The data suggest that UP1/hnRNP A1 may abrogate DNA synthesis arrests at d(GGG) sites by destabilizing the G4′ structure. UP1 does not require NTP hydrolysis energy to unfold the quadruplex as, for example, BLM and WRN helicases do to unwind tetra- or bi-molecular quadruplex DNA [58,59].

9. Destruction of the telomere G4′ structure by binding of UP1

UP1 also binds to $G5_{+TEL}$ and TRM4 $[d(TTAGGG)_4]$, both of which contain four telomeric repeats [52,60]. Under physiological-like conditions, $d(TTAGGG)_4$ also gave a positive CD band at

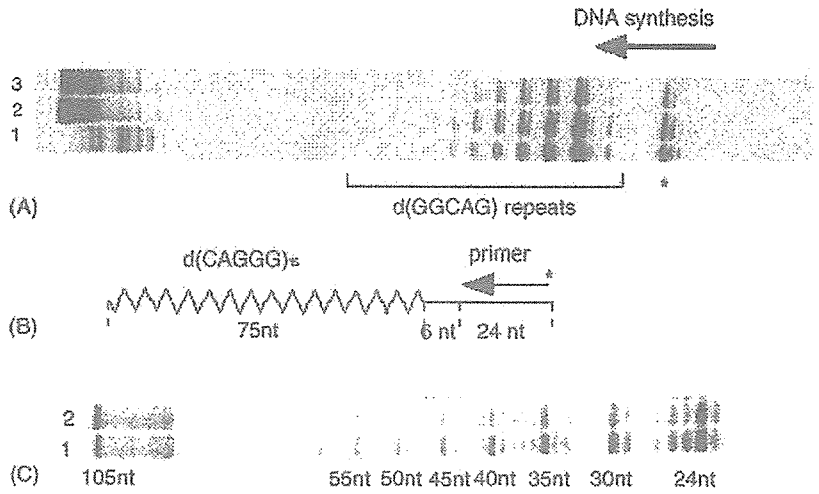

Fig. 4. Effect of UP1 on the arrest of DNA synthesis at d(GGCAG) repeats. (A) Denaturing PAGE analysis of primer extension reactions was carried out with or without UP1 using the single-stranded phagemid pYA-3 carrying $d(GGCAG)_{12}$ as described above (see legend of Fig. 2.) with some modifications [52]. *BcaBEST* DNA polymerase was used for the reaction. Single-stranded pYA-3 with $d(GGCAG)_{12}$ repeat (final 100 nM) in TE buffer containing 100 mM KCl was stored at 7 °C overnight to allow sufficient formation of the quadruplex structure, after heat denaturation at 95 °C for 3 min. Five μl of DNA samples was mixed with 7.5 μl of Milli-Q water and 5 μl of the pUC/M13 (−40) forward primer (Promega) labeled with ^{32}P at the 5′-end (0.5 μM) in TE buffer. The mixture was heated at 60 °C for 7 min and incubated at 37 °C for more than 30 min to allow sufficient quadruplex formation. An aliquot of 1.75 μl of this primer-annealed template (final 23 nM) was mixed with 0.75 μl of 10× *BcaBEST* buffer (200 mM Tris–HCl, pH 8.5/100 mM $MgCl_2$) and 0.5 μl of dNTPs mixture (50 μM each). After addition of 4 μl GST-UP1 suspended in a reaction buffer (20 mM sodium phophate, pH 7.0/0.5 mM DTT), the mixture was incubated at 37 °C for 5 min, and then the primer extension reaction was carried out at 37 °C for 8 min in the presence of *BcaBEST* DNA polymerase (final 66 units/ml). Final concentrations of UP1 added in the reaction are 0 M (lane 1), 6.0 μM (lane 2) and 48 μM (lane 3), respectively. Horizontal arrows indicate the direction of the DNA synthesis, and an asterisk (*) indicates the pausing of the primer extension at d(GGG) present in the multiple cloning sites of the vector plasmid. (B) and (C) A primer extension reaction using a synthetic oligonucleotide pSub15 as a template was performed in the presence and absence of GST-UP1 as described above with some modification. A schematic representation of a 105-mer template pSub15 with $d(CAGGG)_{15}$ repeats used for the primer extension reaction is depicted (B). A mixture of the pSub15 and ^{32}P-labeled M13–20 (Takara) primer (final 100 nM each) was heated in TE buffer containing 150 mM KCl at 95 °C for 5 min and then at 72 °C for 5 min, followed by gradual cooling to room temperature, and stored at 7 °C overnight. The concentrations of *BcaBEST* DNA polymerase, the primer-annealed template, and dNTPs were 18 units/ml, 10 nM, and 1.7 μM, respectively. The concentrations of GST-UP1 were 0 M (lane 1 in (C)) and 750 nM (lane 2 in (C)). Fragment sizes are indicated in nucleotides (nt).

290–295 nm, similar to d(GGCAG) repeats, indicating the formation of a G4′ structure [52]. In contrast, four-stranded parallel quadruplex DNA was not observed except at a much higher DNA concentration (data not shown). In vitro DNA synthesis using synthetic oligonucleotides and several DNA polymerases, including human pol α, was also strongly inhibited at the d(GGG) sites of the telomeric repeats (our unpublished observation). The CD band at 290–295 nm, which is specific for the G4′ structure, was also decreased by addition of GST-UP1 in a dose-dependent manner as in the case of the d(GGCAG) repeats. GST alone did not induce any change in the levels of the band peak [52].

In hnRNP A1-deficient cells, telomere repeats become significantly shorter than in cells with normal levels of hnRNP A1 expression [61]. Restoration of hnRNP A1 expression dramatically increased the average size of the terminal repeat fragment length of the telomere. Interaction of telomerase with hnRNP A1 was also demonstrated by LaBranche et al. [61]. Physical interaction of hnRNP A1, telomeric DNA and human telomerase RNA was also demonstrated by Fiset and Chabot in vitro [62]. These results suggest that hnRNP A1 and its shortened derivative UP1 possibly play a key role in telomere maintenance by destroying the quadruplex structure of the telomere end in vivo. After destruction of the G4′ structure of telomere repeats, telomeric regions may become accessible for telomerase binding, enabling the proper maintenance of telomeres in cells [63].

10. UP1 unfolds the higher order DNA structures of d(CGG) triplet repeats

Another important functional aspect of UP1 is its role in the unfolding the higher order DNA structures of d(CGG) triplet repeats [64]. The $d(CGG)_n$ tract

forms hairpin, quadruplex, and homoduplex structures in vitro under physiological-like conditions [64–66]. In our study, the CD band analysis of $d(CGG)_{16}$ in either the presence or absence of 150 mM KCl showed a large negative peak at 255 nm and a weak positive peak at 280 nm, suggesting the formation of a non-B-type higher order DNA structure (Fig. 5A). The CD spectrum of oligonucleotide CGG16mut, having C to A substitutions at two sites in CGG16, represented a typical pattern of the B structure with comparable negative and positive peaks at 255 and 280 nm, respectively (Fig. 5B). Fragile X syndrome, the most common form of inherited mental retardation in humans, is caused by expansion of a d(CGG) triplet repeat in the 5′-untranslated region of the first exon of the FMR1 gene [67–69]. Although the molecular mechanisms underlying the unstable expansion of the repeats are yet to be elucidated, formation of higher order DNA structures by d(CGG) repeats as described above could be responsible for the induction of genomic instability and the expansion mutation at these repeats.

Several proteins have been identified and reported to unfold or destabilize the higher order structure of $d(CGG)_n$, including WRN helicase [59,70] and two telomeric DNA binding proteins, qTBP42 and uqTBP25 [57]. Here, we demonstrate that UP1 also

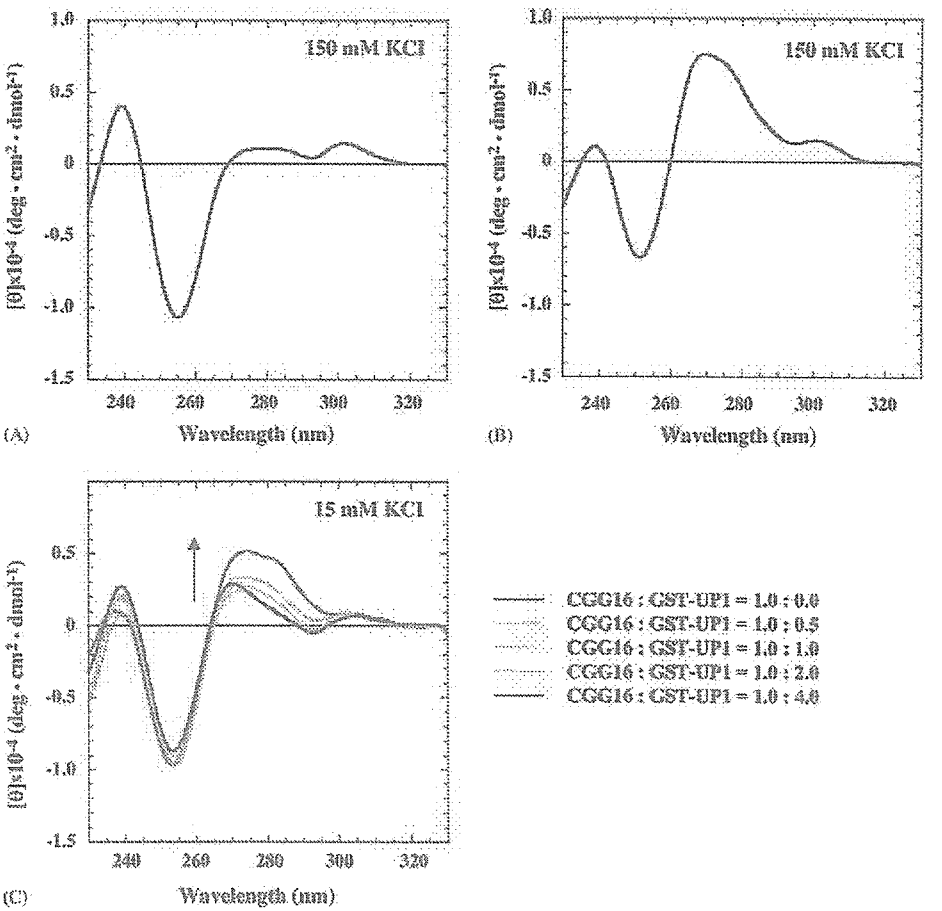

Fig. 5. CD spectra showing the effect of UP1 on higher order DNA structures of the d(CGG) repeat. (A) CD spectrum of $d(CGG)_{16}$ [CGG16] in the presence of 150 mM KCl. A large negative peak at 255 nm and a weak positive peak at 280 nm, which is suggestive of the formation of a non-B-type DNA structure, was observed. CGG16 also gave a similar CD pattern in the absence of KCl (data not shown). (B) CD spectrum of oligonucleotide CGG16mut in the presence of 150 mM KCl. CGG16mut, the sequence being $d(CGG)_5(\underline{A}GG)(CGG)_4(\underline{A}GG)(CGG)_5$, has C to A substitutions at two sites in CGG16. The spectrum represents a typical pattern of the B-structure with comparable negative and positive peaks at 255 and 280 nm, respectively. CGG16mut also showed the B-structure pattern in the absence of KCl. (C) CD spectra of CGG16 titrated with GST-UP1 in the presence of 15 mM KCl, the concentration at which the primer extension reaction was carried out with a synthetic 92-mer oligonucleotide pSubCGG16, containing a d(CGG) repeat, as a template. From each spectrum, the spectrum of the corresponding protein is subtracted, and CGG16:GST-UP1 molar ratios are indicated at the right bottom. Arrows indicate the changes of positive peaks of CD spectra in accordance with increased amounts of added GST-UP1 protein.

binds and unfolds the non-B structure of d(CGG) repeats (Fig. 5C). DNA synthesis is severely obstructed in vitro within the repetitive sequence, similar to the d(GGCAG)$_n$ repeats (data not shown). Addition of molar excess (compared to the template) of GST-UP1 reduces the arrest of DNA synthesis for several DNA polymerases in vitro, including human DNA polymerase α [64].

11. Expression of hnRNP A1 and hnRNP A3 in sporadic human colorectal cancers

Both hnRNP A1 and A3 are over-expressed in human colorectal cancers [71]. In the case of hnRNP A1, quantitative gene expression analysis revealed that 60% (18/30) of sporadic human colorectal cancers showed over-expression of hnRNP A1 in cancer tissues by at least two-fold compared to their normal counterparts. Interestingly, 78% of cases at clinicopathological stage II showed increased expression of two-fold or greater; this is two-fold higher than that seen in the more advanced stage IV [71]. This may imply that the biological impact of hnRNP A1 over-expression is in the relatively early stages of colon carcinogenesis. The over-expression of hnRNP A1 could contribute to the maintenance of telomere repeats in cancer cells and allow enhanced cell proliferation.

12. C-rich strands of minisatellite binding proteins

C-rich binding proteins, LRP130 and Tudor-SN/SND1, were also isolated from OA-treated NIH3T3 cells using oligonucleotide d(CTGCC)$_8$ as a probe, as described earlier [48]. It has been demonstrated that LRP130 and Tudor-SN/SND1 have some sequence specificity for DNA binding [72,73]. Interestingly, both LRP130 and Tudor-SN/SND1 bind to C-rich RNA sequences in a sequence specific manner, and are mainly localized at perinuclear regions and in the cytoplasm [74]. This may suggest the involvement of LRP130 and Tudor-SN/SND1 in RNA metabolism, mRNA transportation and/or specific mRNA transcription of sequences harboring a portion of C-rich residues. At present, we do not have a clear idea of the biological functions of these C-rich DNA/RNA binding proteins. It is possible that these proteins cooperate with hnRNP A1 and A3 (that bind to the G-rich DNA sequences) and exert some novel control of, for example, transcriptional regulation, mRNA metabolism or some other biological pathways.

13. Implication of G4 DNA structures in promoter regions in gene transcription

Although the biological roles of G-rich repeat sequences capable of adopting G4 DNA structures are still largely elusive, one of the intriguing fields of G4 DNA structure research is in its possible involvement in regulation of gene transcription. The G4′-quadruplex structure of the promoter region of the *c-myc* oncogene has been found to function as a transcriptional repressor [75] and the expression of *c-myc* can be inhibited by ligand-mediated G4-quadruplex stabilization [76]. In the case of the human insulin gene, unusual DNA structures of 14 bp G-rich tandem repeats are also thought to affect transcriptional activity, possibly through formation of G-quartets [34,77]. The presence of a guanine-quadruplex forming region within a polypurine tract of the hypoxia inducible factor 1α (HIF1α) promoter was also recently demonstrated; this unusual DNA structure may be involved in regulation of basal HIF-1α expression [78].

14. Future perspectives

G-rich repetitive sequences are frequently observed in the genome and are a subset of triplet repeats and of minisatellite DNA. Because of the peculiar and specific DNA structures adopted by G-rich repetitive sequences, these genomic regions might induce DNA replication fork arrest, leading to size alterations of the repeats in vivo. Various cellular components, such as WRN, TBPs, UP1 and hnRNP A1, may work as guardians against G-rich repeat length instability. In addition, C-rich sequence binding proteins, LRP130 and Tudor-SN/SND1, may cooperate with G-rich binding proteins, and facilitate the resolution of G4′ structures. A fascinating and intriguing scenario for the biological function of these MNBPs is their involvement in transcription of either the G- or C-rich repeat strands. Indeed, most MNBPs isolated from NIH3T3 cells in our own studies as well as by others, bind to mRNA transcripts (data not shown). Binding of hnRNP A1 and hnRNP A3 to G- or C-rich transcripts may affect the transcriptional efficiency and/or the fate of the transcripts of the G-rich region in the genome [40]. Further studies should be conducted to gain more insight into the biological impact of G-rich repetitive sequences, which are widely spread throughout the genome.

Acknowledgements

The authors thank Drs. Minako Nagao and Takashi Sugimura for their helpful comments and continuing